NASA Contractor Report 3543

High Temperature Low Cycle Fatigue Mechanisms for a Nickel-Base and a Copper-Base Alloy

Chin-I Shih

NASA

NASA Contractor Report 3543

High Temperature Low Cycle Fatigue Mechanisms for a Nickel-Base and a Copper-Base Alloy

Chin-I Shih
University of Cincinnati
Cincinnati, Ohio

NASA

National Aeronautics
and Space Administration

**Scientific and Technical
Information Office**

1982

TABLE OF CONTENTS

1. INTRODUCTION

In jet engines and nuclear reactors some of the critical components are invariably subject to fatigue at elevated temperature in hostile environments. To account for those critical design requirements and to achieve maximum utilization of those components without compromise in safety or reliability, it is necessary to be able to predict the life of the system. So far a major difficulty in life prediction lies in the uncertainty associated with the effects of creep and environmental attack at high temperature. The relative importance of these effects and how to incorporate them into a life-prediction scheme are still not well understood at the present time.

A number of models has been proposed to date for predicting fatigue life at elevated temperature. To name a few well-known ones, we have strain-range partitioning model (SRP),[1] frequency separation model (FS),[2] Ostergren model[3] and damage rate model (DR).[4] Traditionally, these models have been formulated based on intuitive hypothesis of what constitutes damage. The fatigue life is then experimentally determined in terms of chosen parameters. Mechanisms of damage accumulation dealing with high temperature low cycle fatigue (LCF) have also been discussed from a metallurgical point of view.[5,6] It is recognized that numerous damage mechanisms can occur as a result of a number of factors like **plastic deformation,** creep deformation, creep/plastic interaction, environmental effects, development of new phases and interactions amongst the above factors.[6] Because of the complexity of the damage accumulation pro-

cess, which, realistically is a function of material, loading conditions, temperature and environment, it may be incorrect to use any particular mode listed above to describe it. The existing life prediction models, have been applied to several materials with promising results. However, the applicability and limitations of these models need to be evaluated for materals used in aerospace industries.

The main purpose of this study is to determine the mechanism controlling deformation and failure under cyclic conditions of two materials for aerospace applications. The first one, nickel-base superalloy Rene'95, is used in the manufacture of turbine disks. The second one, copper-base alloy NARloy Z, is a candidate material for rocket nozzle liners in engines of space shuttle, orbit-to-orbit shuttle and space tug etc. These two materials have quite different microstructures and mechanical properties. Presumably they also will have different damage accumulation mechanisms and their lives will be described by different fatigue models.

2. REVIEW OF LITERATURE

The problem of fatigue at elevated temperature is basically one
of cumulative damage. This involves some fatigue mechanisms governed
by cyclic strain in conjunction with some creep mechanisms and/or cer-
tain mechanisms involving only environmental effects. In some cases,
metallurgical changes (morphological changes in existing phases, deve-
lopment of new phases etc.) are also treated as sources of damage that
may interact with the above mechanisms and degrade the fatigue life.
The effect of creep and environment generally becomes increasingly
important with increases in temperature and/or decreases in strain
rate (frequency) and also when hold time is introduced to each cycle.
Eventually fatigue at high temperature is, in fact, a time dependent
process that is a function of the material, strain (stress) range,
cycle type and environment.

2.1   Damage Mechanisms of High Temperature Fatigue:

Frequently, the fatigue process is discussed in terms of
crack initiation and propagation stages. At high temperature, the
nature of these two stages is completely dependent on the damage
mechanisms cited above and consists of the overall microscopic aspect of
fatigue fracture phenomenon. It is, therefore, appropriate to con-
sider briefly the two main stages of crack initiation and propagation.

2.1.1   Transgranular Crack Initiation and Propagation:

The transgranular crack initiation stage can be correlated
quite well with the deformation character of the material.[7] In the

case of planar slip, dislocations are confined to glide in individual slip planes giving rise to heterogeneous deformation such that dislocations pile up against barriers like grain boundaries, incoherent precipitate particles etc. This causes strain localization in the slip bands and cracking along slip planes eventually takes place. This type of deformation is favored under conditions of low stacking fault energy (SFE), low temperature, low strain and the presence of coherent precipitates. Fracture along 45° plane to the stress axis and a slight change in the direction of crystallographic fracture facets with orientation are typical of this type of cracking. This is generally referred to as stage I cracking. For planar slip materials, the degree of slip homogeneity is important in determining the rate of slip band crack initiation and propagation.

For wavy slip, the dispersal of slip to adjacent slip planes by means of dislocation cross slip and climb leads to homogeneous deformation. This results in transgranular cracking that is macroscopically perpendicular to the stress axis. It is referred to as stage II cracking. This type of deformation is favored by conditions like high SFE, high strain, incoherent precipitates and most importantly, temperature greater than 0.3 - 0.5 T_m where T_m is the absolute melting point. The influence of temperature is very important because thermal activation assists slip dispersal. In many high temperature alloys crack initiation is governed by second phase particles or defects. Similarly, twin boundaries affect crack initiation in wrought materials. The crack can initiate at inclusions[8,9] or

carbides,[10,11] at micropores,[9,11] between carbide/matrix interface[12] or along coherent annealing twins.[13,26]

Generally transgranular crack propagation is favored at low temperatures. Low mean stress and high frequency render it favorable at elevated temperature. It can be either stage I or II mode depending on the nature of deformation at the crack tip. The mechanisms of both modes involve crack growth by localized deformations essentially from a plastic blunting process[14] or by the accumulation of damage at the crack tip - a micro LCF process.[15] The striations observed in stage II of ductile materials such as stainless steels and OFHC copper at elevated temperature are developed first by the plastic blunting of the cracktip during the tension part of the fatigue cycle followed by resharpening of the crack in the compression part. But in materials with low ductility such as nickel-base superalloys, marked striations are not seen very often.[13] A crack initiated in stage I will change to stage II when it gets to a certain length and encounters a grain boundary. This length is a function of strain and frequency.

2.1.2 Intergranular Crack Initiation and Propagation:

For most materials, intergranular cracks can be developed during fatigue under conditions of lower strain rate and temperatures above $0.5 \ T_m$. This phenomenon is mostly due to the effect of creep. The creep effect is visualized as either a process of nucleation and growth of cavities or triple point cracking. Both these processes have been discussed in great detail for the case of creep under static

loading. Only recently, Veevers and Snowdown[16] have reviewed the role of these processes in fatigue.

It is generally believed that grain boundary sliding (which was experimentally shown to be controlled by intragranular deformation[17,18]) is responsible for intergranular cracking. For single phase alloys cavitation is observed to be associated with grain boundary sliding. This grain boundary sliding is enhanced when the boundaries tend to align themselves at 45° to the stress axis through migration during cycling. The cavity density exhibits a maximum when the boundaries are so aligned.[19] Once the cavities are initiated, they are still thermodynamically unstable unless they attain a critical size. There is sufficient experimental evidence to prove that vacancies produced by cyclic plastic deformation can stabilize the cavities.[20,21]

The maximum cavity population on the boundaries aligned at 45° to the stress axis was also seen in systems where grain boundary sliding is restricted by particles at the boundaries.[20,21] Raj[22] proposed that this is due to stress concentration at grain boundary precipitates. Intergranular cracks are often initiated at the interface between grain boundary particles and the matrix.[23,24] The exact mechanism is still not understood at the present time. Wells et al.[7] believe that impediment of grain boundary sliding is attained when the particle-matrix interface is more strongly bonded than the misoriented matrix and the particles are equiaxial and are relatively wide spaced. Experimental results suggest that there is an optimum

size and volume fraction of grain boundary precipitates which will resist grain boundary sliding and cavitation.[25,26] It has been observed that blockage of slip bands and twin boundary shear can assist intergranular crack initiation through particle-matrix interfacial separation[27] or grain boundary ledge formation.[28,29] This mechanism, in addition to stage I cracking cited in transgranular initiation, becomes most important when slip is planar and heterogeneous.

Triple point cracks are described by the Stroh model[30] as those occurring by the build-up of stress intensity at a triple point before the deformation within grains or along the boundaries can provide sufficient relief. Because it requires large shear offsets at the triple point, this type of cracking should be enhanced by large strain ranges and cycles containing a creep hold.

Tensile hold time studies on austenitic stainless steels revealed significant differences in fracture morphology and in life as compared to combined tensile and compressive holds.[31-33] Fractures in the former case were largely intergranular. Addition of even short compression hold times causes essentially transgranular fracture and increases life. It is believed that tensile half cycle produces both cavities and triple point cracks. Further, it also accelerates their growth. The compressive half cycle, on the other hand, not only retards their growth but also tends to heal them by reversed grain boundary sliding. Similarly, a degradation in life and change in fracture morphology were seen in unsymmetrical strain rate cycling slow-fast tests,[34] as compared to symmetrical strain rate cycling. A

mechanism involving fracture of grain boundaries by triple junction cracking in the crack tip region was proposed by Min and Raj.[35] They derived a critical tensile going strain rate (where the boundaries can slide just fast enough to keep up with the rate of deformation) below which grain boundary sliding (intergranular damage) occurs.

2.1.3   Effect of Environment:

It has been recognized for some time that the environment can seriously affect fatigue properties especially at elevated temperature. Coffin[36] investigated this for AISI 304 by testing at high temperature in vacuum and at room temperature in air and compared his results with the observations of Berling et al.[37] at high temperature in air. It was noted that room temperature behavior could be produced by testing at high temperature in vacuum. According to Coffin[36] since in vacuum the effect of environment can be isolated readily, the life degradation in air was found to be mostly due to environmental effect. However, care should be taken when interpreting the results of tests done in vacuum. Though environmental effects are absent, thermal etching of grain boundaries due to the presence of elements with a high vapor pressure can cause early intergranular cracking. Coffin[38] also studied LCF of A286 over the frequency range 5 to 0.1 cpm . He noted a pronounced frequency dependence and intergranular cracking when the tests were run in air. In contrast, tests run in vacuum exhibited transgranular cracking and did not show such a frequency effect. This led to the conclusion that in this frequency range, environmental effects were responsible for the frequency dependence as

well as enhancement of intergranular fracture.

McMahon and Coffin[39] examined the fatigue results for cast Udimet 500 tested in air and found that localized oxidation is important to the failure process. Life degradation was more a result of "oxidation" fatigue (analogous to corrosion fatigue) than due to creep damage processes. Because chemical segregation and more open structure render them more susceptible to oxidation, grain boundaries are preferentially attacked by the environment.[40] Pre-oxidizing Udimet 700 specimens at 982°C followed by fatigue testing at 760°C produced many surface integranular cracks, whereas testing without prior oxidaton produced a single intergranular crack.[41] Thus pre-oxidized or preferentially oxidized grain boundaries serve as incipient cracks.

Oxidation can sometimes be beneficial to fatigue also. It may retard crack growth by increasing the cracktip radius and reducing the amount of crack resharpening in compression[42,43] This role of oxide in crack blunting was also reported in creep to explain the longer stress rupture lives in air than in vacuum.[44] Exact mechanisms associated with environmental effects are still not well understood at the present time.

2.2   Fatigue Behavior of Nickel Base Superalloys:

Nickel-base superalloys have low SFE fcc matrix(γ) that are strengthened through solid solution, second phases (γ ',γ ",oxides) and various metallic carbides.[45] As a consequence, they possess excellent resistance to fatigue and creep. In addition, these superalloys have good corrosion and oxidation resistance. These pro-

perties are essential to high temperature applications in jet engines.

Fatigue behavior of nickel-base superalloys has been extensively studied at both ambient and high temperatures. In these alloys at low temperatures and high frequencies, slip is planar. Depending on its size, γ' is either sheared or looped by dislocations.[46] As a result, stage I cracking along slip band is the predominant initiation mode. This has been observed in Udimet 700 by Wells et al.,[47] by Merrick[26] in Waspaloy, Inconel 718 and Inconel 901, in Astroloy by Runkle,[25] in Udimet 710 by Moon et al.,[48] and by Leverant et al.[49] in Mar-M200 single crystal. Stage I initiation was also found at defect sites by Gell et al.[42] in Mar-M200 and by Menon et al.[50] in Rene' 95.

Duquette et al.,[51] found that air environment had a profound influence on stage I cracking in Mar-M200 single crystal at room temperature. They explained its shorter fatigue life in air in terms of the reduction in surface energy at the stage I crack tip due to oxygen adsorption.

Studies on Rene' 95[52] and Waspaloy[53] by Antolovich et al. on Astroloy by Merrick et al.[54] and on IN 718 by Mills et al.[55] showed that their fatigue crack propagation (FCP) behavior is improved by a microstructure that promotes slip planarity. In transgranular mode, an increased slip planarity accelerates stage I cracking, but tends to lower the fatigue propagation rate (FCPR) when oxidation effect is only minor. In the temperature range of 550° to 650°C, however, Clavel et al.[56] observed greater frequency dependence of FCPR in Inconel 718 than in Waspaloy due to the occurrence of intergranular

cracking. The deformation in Waspaloy was rather homogeneous while in Inconel 718 it was very heterogeneous and planar. This led them to conclude that the occurrence of intergranular fracture at high temperature in these two alloys is favored by heterogeneous deformation (planar slip). This fact can be explained by the grain boundary cracking due to the blockage of slip bands, as later observed by Lerch[57] in Waspaloy.

A transition from stage I to stage II cracking in fracture path is often observed in nickel-base superalloys[13,25,26] without a change in slip character. Pelloux et al.[25] think that the transition is governed in part by the ratio of reversed cyclic plastic zone size R_c^p at the crack tip to the grain size d. They suggested that for small R_c^p/d, the crack tip opening is accommodated by Mode II displacement along stage I cracks. As R_c^p becomes larger than d, plastic deformation at the crack tip becomes more typical of continuous plasticity and stage II cracking begins. A change to stage II cracking was also observed by Leverant and Gell[49] in Mar-M200 at elevated temperature. They however relate that to a change in deformation such as slip becoming wavy.

At a temperature greater than 0.5 T_m, (the actual temperature depends on strain rate or frequency), cracking during fatigue frequently becomes intergranular. Wells et al.[47,58] showed that in Udimet 700 the surface cracking is intergranular at 760° and 926°C as opposed to stage I at room temperature. Also they noted that at elevated temperatures void initiation and coalescence were the rate

controlling mechanisms. Fatigue studies on Udimet 500 and Rene' 80 by Coffin et al.[39,59] revealed that intergranular oxidation is the primary mechanism of crack initiation at 871°C. While the cracking remained intergranular in Udimet 500, the fracture path changed to stage II after one grain diameter in Rene' 80. Antolovich et al.[60] also studied Rene' 80 with prior exposure under stress and found a large reduction in fatigue life. They concluded that the most severe form of damage was associated with environmental interactions in the boundaries.

The effect of air environment on the high temperature FCP for nickel-base superalloys has also been reported in the literature.[61] In general, its effect on the FCP is to increase the crack growth rate. The environment can, sometimes, promote intergranular cracking, particularly when there is a decrease in frequency.

Hold time and frequency are found to have a significant effect on fatigue behavior of nickel-base superalloys.

2.2.1   Effect of Hold Time:

In austenitic stainless steel most damage was observed with tensile hold.[31,33] From a study of Udimet 700 at 760°C with interspersed dwell times, Wells et al.[27] noted that compressive dwells were more harmful than tensile ones. The reason for this was speculated to be the flatter shape of grain boundary voids and a greater crack tip stress intensity when compressive holds were present. Hold time studies by Coffin[62] in LCF of Rene' 80 at 760°C showed that compressive hold is more damaging than tensile hold. He

argued that a tensile hold accompanied by compressive mean stress is beneficial to fatigue resistance and that compressive hold with tensile mean stress acts to reduce the fatigue life. A similar observation was also made by Feranish and McEvily[63] with 2.25 Cr-1 Mo steel. They related the observed behavior to combined interactions of oxide formation, spalling and surface deformation. In compression following a tension hold the oxides spall to produce a new surface free of macroscopic cracks while in tension following a compression hold the oxides crack instead, creating localized stress concentrations that facilitate crack nucleation.

Sadananda and Shahinian[64-66] studied FCP in Inconel 718 and Udimet 700 and concluded that hold time effects depend on two factors; environmental effects in relation to creep effects, and applied stress intensity at the hold period in relation to threshold stress intensity for creep crack growth K_{thc}. If the applied stress intensity during a hold time is greater than K_{thc}, then hold time increases crack growth rates due to both environmental and creep effects. If the stress intensity is less than K_{thc}, environmental effects could still accelerate crack growth if the creep deformation rate is sufficiently low. But if the rate is high enough then crack tip blunting occurs which arrests crack growth in spite of the environmental and cyclic effects.

2.2.2   Effect of Frequency:

Organ and Gell[43] observed that fatigue life in Udimet 700 tested at 760°C increased first as frequency increased from 2 to 600 cpm but decreased at 6×10^4 cpm. They suggested that there were two

competing effects with increase in frequency. The increase in life at first was because of the greater tendency to eliminate the effects of creep and oxidation, thereby changing crack initiation from intergranular to stage I. The reduction in life later was on account of predominant effect of increasing slip planarity which, in fact, accelerated stage I cracking. In the case of Rene' 80, Antolovich et al.[67] observed that at 871°C and 982°C with the damage controlled by environmental effects, life increased with decreasing strain rate from 50 to 0.5 percent min^{-1}. This was attributed to 'coarsening which was beneficial in as much as it increased the ductility.

2.3   Damage Mechanisms in Rene' 95:

Rene' 95 is a high-strength wrought nickel-base superalloy, developed by General Electric Co.[68] It has high potential for application in the manufacture of compressor and turbine disks in advanced aircraft engines. Like other nickel-base superalloys, Rene' 95 is strengthened by γ' precipitation $[Ni_3(Al,Ti,Cb)]$ and solid solution lattice strain from the addition of Mo, W, Co and Cr to γ' matrix. The carbides, act to prevent grain boundary sliding (creep damage) is in the form of MC $[(Ti,Cb,W)C]$. The total weight percentage of γ' forming elements (Al, Ti and Cb) is 9.5 - the number from which the alloy derives its name.

A special thermomechanical processing,[69] involving warm working the alloy in the two phase $\gamma - \gamma$' region at a temperature below that of rapid recrystallization, imparts in Rene' 95 a duplex microstructure, that consists of large warm-worked grains surrounded

by a fine grained recrystallized "necklace". Shamblen et al.[70] found that in the range 538°C to 650°C, Rene' 95 with duplex microstructure possesses mechanical properties superior to those of the same alloy processed in the conventional way, having one hundred percent fine grain structure. They ascribed this to greater crack propagation resistance in air of the duplex structure by virtue of its large warm worked grains.

Previous studies on tensile and fatigue deformation behavior by Menon and Reimann[71,50] showed a more homogeneous deformation mode for necklace Rene' 95, as compared to the coarse planar mode occurring in conventional superalloys. They believe that dislocation substructure in the warm-worked grains is very effective in dispersing slip throughout the grain, thus forcing the material to deform homogeneously. They further suggest that the presence of necklace grains is also responsible for such homogeneous nature of deformation. Microtwinning[72] has also been observed as a mode of deformation during tension and fatigue. The same authors suggested that it is associated with the residual dislocation substructure in the warm-worked grains.

In their LCF and creep study, Menon and Reimann[50,73] found that the presence of MC carbides affects crack initiation of Cast + Forged Rene' 95. At ambient temperatures crack initiation associated with cracking or decohesion of MC carbides appeared to make fatigue life shorter than that due to only slip band cracking. At 650°C the presence of MC carbides that had undergone partial decohesion from the

fracture surface was seen near the stage I area. Typically the fracture surface consisted of both stage I and stage II regions. Creep results at 650°C in air showed higher minimum creep rates, shorter steady state creep periods and lower rupture lives as compared to those in vacuum. It was shown that air tested specimens with MC carbides on the surface were prone to surface cracking. Cracks generally initiated and propagated intergranularly along the necklace region. In contrast, specimens tested at 650°C in vacuum were not prone to surface carbide cracking any more than when the carbides were inside the specimen. The authors did not see any evidence of the propagation of a single crack. Instead, they observed a mixture of intergranular cracks and dimple rupture. These results demonstrate the strong environmental effect on creep crack initiation in Rene' 95. Bashir et al.[9] studied LCF of HIP + Forged PM Rene' 95 in air and found that a great enhancement in life was associated with subsurface initiation. This led them to conclude that there is a very significant environmental effect on the LCF of Rene' 95 at 650°C. They indicated that the fatigue life based on plastic strain was at least as great with tension hold time as for continuous cycling, and crack propagation tends to occur by a boundary mechanism at least initially. As for continuous cycling, cracking always changed from transgranular to intergranular. The transition was described in terms of a critical combination of crack length and strain.

2.4   Damage Mechanisms in NARloy Z and Pure Copper:

NARloy Z is an alloy of copper with slight addition of

silver and zirconium. This alloy was specially developed by Rockwell North America Inc.[74] to meet the requirements of high thermal conductivity and fatigue resistance for rocket nozzle liners. By the addition of Zr to Cu-Ag alloy, uniform continuous precipitation, refined grain size and improved ductility are attained. NARloy Z being a proprietary material, there is no published report in the literature of its fatigue behavior. However, literature on fatigue characteristics of pure copper at elevated temperature is available.

Wigmore and Smith[75] studied LCF behavior of oxygen-free. high conductivity (OFHC) copper between 400° and 600°C. They noted the occurrence of grain boundary sliding and grain boundary migration that produced preferential orientation of boundaries at 45° to the stress axis. Cracking was found at triple points as a result of stress concentration induced by grain boundary sliding. The cracks increased in length with further fatigue and eventually link together by ductile rupture causing final failure. Similar observations were reported by Abdel-Raouf et al.[76] in OFHC copper at 650°C. They did not see any migration at 300°C. Testing vacuum-cast copper (which has a slightly higher purity level than OFHC copper) under the same conditions, Wigmore and Smith[75] observed no triple point cracking. Final failure was from what the authors identified as plastic instability effect. Sidey and Coffin[77] tested OFHC copper at 400°C at unequal strain rates to study the effects of wave shape. The fatigue lifetime decreased by an order of magnitude as the tensile going strain rate was reduced from 1.7×10^{-3} s^{-1} to 1.7×10^{-5} s^{-1} at

constant cyclic period. Accompanying this reduction in lifetime was a change in fracture mode from transgranular in the case of fast-slow tests to intergranular (internal cavitation) for slow-fast tests.

2.5 Fatigue Life Prediction Models:

Criteria for life prediction is generally established in two ways: (a) by consideration of cyclic and time-dependent effects as separate phenomena, and combining the damage function by assuming a linear damage accumulation rule, for each determined separately as in the SRP model; or (b) by consideration of the cyclic and time effects as a single process expressed in terms of several variables, including the strain rate or frequency of the cycle as in FS, Ostergren and DR models. Each of these models is discussed in the following sections.

2.5.1 Strain-Range Partitioning Model:

The strain-range partitioning (SRP) concept[1,78] is an extension of the Coffin-Manson law (which is valid at room temperature) to high temperature by including the interaction of time-dependent inelastic strains (creep) and time-independent inelastic strains (plasticity). The inelastic strain range consists of four components, $\Delta \varepsilon_{pp}$, $\Delta \varepsilon_{pc}$, $\Delta \varepsilon_{cp}$, $\Delta \varepsilon_{cc}$. From these, four inelastic strain-life relationships are constructed. Then the interactive law in the following form is invoked;

$$\frac{F_{pp}}{N_{pp}} + \frac{F_{pc}}{N_{pc}} + \frac{F_{cp}}{F_{cp}} + \frac{F_{cc}}{N_{cc}} = \frac{1}{N} \tag{1}$$

where F_{ij} = fraction of the ij inelastic strain component

N_{ij} = life calculated from the pre-determined strain-life

relation of ij assuming all of the inelastic strain

to be of the component of interest.

N = predicted overall life.

It should be noted that except for the $\Delta\varepsilon_{pp}$ vs N_{pp} curve all other relationships are computed assuming that eq. (1) is valid. Clearly this introduces an element of redundancy into the scheme.

The applicability of the SRP model was demonstrated with the following systems: AISI 316 at 705°C, 2.25 Cr-1Mo steel, A286 and H-13 steel at 595°C, Incoloy 100 at 925°C, T-111 at 1150°C.

2.5.2   Frequency Separation Model:

Modifying the Coffin-Manson law by introducing a frequency term to account for a creep effect, Coffin[34] proposed an expression,

$$\Delta\varepsilon_p \, (N_f \, \nu^{k-1})^\beta = C \tag{2}$$

This modification though it incorporates time dependence factor, is inadequate to account for the behavior of unbalanced loop. This is resolved in the frequency separation (FS) model,[2] by application of the elastic strain and life relationship.

$$\Delta\varepsilon_e = \frac{\Delta\sigma}{E} = A \, \Delta\varepsilon_p^{\,n} \, \nu^{k_1} = A'N_f^{-\beta'} \, \nu^{k_1} \tag{3}$$

and determination of the stress range of unbalanced loops by

$$\Delta\sigma_{SF} = \Delta\sigma_{FS} = \frac{A}{2} \left[\left(\frac{\nu_c}{2}\right)^{k1} + \left(\frac{\nu_t}{2}\right)^{k1} \right] \Delta\varepsilon_p^n \qquad (4)$$

The cyclic life is then determined from

$$N_f = \left(\frac{A'}{\Delta\sigma_{SF}}\right)^{1/\beta'} \left(\frac{\nu_t}{2}\right)^{k1'/\beta'} \qquad (5)$$

where $\Delta\sigma_{SF}$ = stress range of a slow-fast loop

$\nu_t/2$ = tension-going frequency

$\beta' = n\beta$

$k_1' = k_1 - (k-1)\beta'$

A more general form which incorporates plastic range, tension going frequency and the loop time balance as important variables, is given by

$$N_f = D\Delta\varepsilon_p^a \; \nu_t^b \left(\frac{\nu_c}{\nu_t}\right)^c \qquad (6)$$

It should be noted that the stress range in eq. (4) is really a fictitious term which, is, in reality, determined from two experiments.

Examples of systems with successful application of FS model are AISI 304 at 593°C; and AISI 316 at both 566°C and 704°C.

2.5.3 Ostergren Model:

Ostergren[3,79] considered LCF to be essentially a problem of crack propagation and assumed that only the deformation which occurs when the crack is open contributes to crack propagation and thus to

fatigue damage. A damage function $\sigma_T \Delta \epsilon_p$, proportional to the net tensile hysteretic energy, was then introduced as a measure of damage. This results in an equation

$$\sigma_T \Delta \epsilon_p N_f^\beta = C$$

similar to Coffin-Manson law. In order to account for hold time and frequency effects on life, time-dependent damage equation was developed, similar to Coffin's frequency modified equation:

$$\sigma_T \Delta \epsilon_p [N_f \; \nu^{(k-1)}]\beta = C \tag{7}$$

For time-dependent, wave shape independent condition, the frequency is the inverse of the cycle period $\nu = 1/(\tau_0 + \tau_t + \tau_c)$, whereas in the case of time-dependent, wave shape dependent situation, $\nu = 1/(\tau_0 + \tau_t - \tau_c)$ and $\nu = 1/\tau_0$ for $\tau_t \leq \tau_c$. In terms of mechanisms, in the former case, it hypothesizes that time dependent damage results primarily from environmental reacitons (oxidation), while in the latter case, it accounts for the greater time-dependent damaging effect of unreversed tensile creep deformations.

Systems to which Ostergren model is applicable are IN 738 and Rene' 80 at 871°C (time-independent); Cr-Mo-V at 538°C (time-dependent, wave shape independent) and AISI 304 at 538°C (time-dependent, wave shape dependent).

2.5.4 Damage Rate Model:

The damage rate model[4,80] assumes that LCF is primarily a process of propagation of pre-existing microcracks and the crack

growth rate da/dt is governed by the strain and strain rate as follows:

$$\frac{da}{dt} = \begin{array}{l} aT|\varepsilon_p|^m |\dot{\varepsilon}_p|^k \quad \text{(under tensile stress)} \\ aC|\varepsilon_p|^m |\dot{\varepsilon}_p|^k \quad \text{(under compressive stress)} \end{array}$$

$$(8)$$
$$(9)$$

T, C, m and k above are material parameters that are functions of temperature strain rate, environment and the metallurgical state of the material. Usually the transition in these parameters is associated with transitions in the fracture morphology, e.g. from a predominantly transgranular to a predominantly intergranular mode. Cyclic life is obtained by integrating the above equation under the given boundary conditions. For continuous cycling, the following expression is obtained:

$$N_f = [(m+1)/4A] (\Delta\varepsilon_p/2)^{-(m+1)} (\dot{\varepsilon}_p)^{1-k} \tag{10}$$

where $A = (T+C)/2 \, \ell n(a_c/a_0)$

For hold time tests, it is

$$1/N_f = [4A/(m+1)] (\Delta\varepsilon_p/2)^{m+1} (\dot{\varepsilon}_p)^{k-1} + |\varepsilon_{p_{max}}|^m \tag{11}$$

$$\int_0^{t_H} [2A/(1+C/T)] |\dot{\varepsilon}_p|^k dt + |\varepsilon_{p_{min}}|^m$$

$$\int_0^{t_H} [2A/(1+T/C)] |\dot{\varepsilon}_p|^k dt$$

This model has been successfully applied to AISI 304, AISI 316, Incoloy 800 and 2.25 Cr-1Mo steel at various temperatures.

2.5.5 Antolovich's Oxidation Model:

Assuming that there is a combination of environmental penetration and stress at which a microcrack can form, Antolovich[67,81] proposed an oxidation model which can be basically expressed in terms of the equation:

$$\sigma_i^{max} \cdot \ell_i^p = Co$$

where σ_i^{max} = maximum stress at initiation

ℓ_i = oxygen penetration at initiation

p, Co = material constant

Further, the oxygen penetration for an initiated crack may be computed assuming that parabolic kinetics are obeyed:

$$\ell_i = \alpha \sqrt{Dt_i}$$

where α = geometric constant

t_i = time to initiation

D = diffusion constant

The applicability of this model can be examined by taking the time for crack initiation in a given test and comparing it to the shortest crack initiation time for a given set of tests:

$$\ell_i / \ell_i^\circ = (t_i / t_i^\circ)^{1/2}$$

where ℓ_i° = initiation crack length for shortest test

t_i° = time corresponding to ℓ_i°

In applying the oxidation model successful correlations have been obtained from systems: Rene' 80 at 871°C and 982°C, Rene' 77 at 929°C, on Nimonic 90 and Mar-M002 at various temperatures.

3. EXPERIMENTAL

3.1 Materials and Test Procedure:

All the specimens used in this study had already been tested by Mar Test for the AGARD SRP program. The Rene' 95 specimens were tested under the direction of Air Force Materials Laboratory and the NARloy Z specimens under the direction of NASA Lewis Research Center. A brief description of the treatments and testing procedures, as reported[82,83], is given below.

3.1.1 Materials Processing and Heat Treatment:

The chemical compositions and tensile properties of both materials are summarized in Tables I and II. Vacuum induction melted and vacuum arc remelted Rene' 95 ingot about 22.8 cm in diameter was given a homogenization anneal in the range 990°C to 1163°C for 3 hours and then furnace cooled. Two pancakes taken from the ingot were forged in the temperature range 1043°C to 1137°C to reduce them to about 40-50 percent above the final thickness. This was followed by a recrystallization anneal at 1163°C for one hour and cooling to 900°C at a rate greater than 93.3°C per hour. This results in uniform grains varying in size between 0.064 and 0.127 mm. Final reduction was done on these forgings at 1080°C to 1109°C. This imparts sufficient deformation to produce dynamic recrystallization or the "necklace" in the grain boundary region and a heavy dislocation density in the recrystallized grains. They were then partially solution treated at 1093°C and aged at 760°C for 16 hours to produce a γ'

structure in the maxtrix. Specimens were taken in the tangential direction of the pancake.

NARloy Z was furnished in the centrifugally cast form. Following hot rolling it was solution annealed at 927°C and aged at 482°C to let second phases precipitate out. The final material was in the form of a rectangular bar, 23.2 cm long x 5.1 cm x 4.1 cm.

3.1.2   Test Procedures:

Hourglass specimens with both buttonhead and threaded ends shown in Fig. 1(a),(b) were used. The latter were whole Rene' 95, while the former were frictionally welded with Inconel 718, 1.27 cm away from the buttonhead. Low cycle fatigue tests were conducted in air at 650°C, using a servo-hydraulic testing machine. For each test, diametral strain was controlled and then converted to total axial strain which was reported. All testing was done in a fully reversed mode (R_ε = -1, A_ε = ∞ , where R_ε = maximum strain/minimum strain; A_ε = strain amplitude/mean strain). To test the SRP model for high temperature LCF, the test types were designed as shown in Fig. 2. Continuous cycling tests were run at frequencies of 20 and 0.05 cycles per minute (cpm), using triangular waveform. For cyclic strain hold tests the ramp rate was the same as for 20 cpm tests while the maximum strain was held for either 1 or 10 minutes under tension (cp), compression (pc) as well as tension-compression (cc). The strain and stress waveforms for these tests are shown in Fig. 3. In cyclic creep tests, the load was ramped to a prescribed value and was then held allowing the specimen to creep to a fixed diametral strain

limit before reversing the load. In unequal frequency (strain rate) tests, slow-fast tests were carried out at frequencies of 0.05 and 20 cpm for tensile going and compressive going modes respectively. For fast-slow tests the reverse scheme was employed.

Threaded hourglass specimens shown in Fig. 1(c) were used in the study of NARloy Z. All tests were performed at 538°C in high-purity argon (oxygen content less than 0.01 percent by volume) chamber. 3000 ppm of hydrogen was added to provide a slightly reducing environment for additional protection of the specimens. Testing procedure was the same as cited above for Rene' 95. The test matrix was also the same with the exclusion of cyclic creep tests. The strain rates used in continuous cycling tests ranged from 0.004 to 1.0 percent sec^{-1}. For hold time tests the dwell period was 5 minutes. In unequal strain rate tests, strain rates employed were 1/0.04, 0.04/1, 0.004/1 and 0.0007/1 percent sec^{-1} (tension going/compression going).

3.2 This Investigation:

In this study, detailed metallographic examinations were done on selected specimens of Rene' 95 and NARloy Z tested under continuous cycling and with strain hold times. The total strain ranges for Rene' 95 were from 1.8 percent to 0.9 percent. For NARloy Z strain ranges were 2.6 percent and 0.9 percent.

3.2.1 Scanning Electron Microscopy (SEM):

Failed specimens were cut near the fracture surface after ultrasonic cleaning in acetone. The fracture surface and gage section

were examined with a 25 KV Cambridge Steroscan 600 SEM to characterize initiation sites, mechanisms of crack advance and formation of secondary cracks.

3.2.2   Metallography:

Following SEM examination the gage portion was sectioned longitudinally through planes containing the initiation sites and the specimen axis.   These longitudinal sections were cold mounted with addition of the Alumina to the epoxy to prevent the occurrence of round edges during polishing.   Standard techniques were used for metallographic preparation.   Polished Rene' 95 specimens were either chemically etched with Kalling's reagent (2g $CuCl_2$, 12 ml HCl (37% concentration) 180 ml ethanol) or electroetched with a solution of 45 percent acetic acid (99.7% concentration), 45 percent butyl cellusolve and 10 percent perchloric acid (70% concentration) at 20°C and 3V in Buehler polishing unit.   The specimen surface in reaction with the solution is a circle with 1 cm in diameter.   NARloy Z specimens were etched either with 5g $FeCl_3$, 15 ml HCl and 100 ml ethanol after polishing or by adding several drops of NH_3OH (29% concentration) to 0.05 µ Alumina polishing abrasive.   Etched specimens were then examined with optical microscope/SEM to determine the nature of secondary cracking, to detect internal cavitations and to evaluate the importance of carbides and intermetallic compounds on microcrack formation. The same techniques were also used to characterize the initial structure of both materials.

3.2.3 Transmission Electron Microscopy (TEM):

Small wafers were cut perpendicular to the specimen axis as close to the fracture surface as possible. These wafers were electropolished by standard twin jet technique into thin foils. Mixture of 250 ml methanol, 12 ml perchloric acid and 150 ml butyl cellusolve was used in electropolishing Rene' 95 at -30°C and 30V. For NARloy Z a solution mixture of 100 ml HNO_3 (70% concentration) and 200 ml methanol was used at -25°C and 15V. The foil surface in reaction with the solution is a circle with 3 mm in diameter. The low temperature was attained by using a Cryscool cooler. These thin foils were examined with a 200KV JEOL JEM-200A TEM to characterize the detailed microstructure and the deformation behavior of each system.

4. RESULTS AND DISCUSSION

4.1   Rene' 95:

4.1.1   Initial Structure:

The microstructure of Rene' 95 forgings has been characterized earlier by Menon.[84] The undeformed structure of as received Rene' 95 specimens observed in this study was the same as reported by Menon.

Fig. 4 shows the typical necklace structure of Rene' 95. The warm worked grains of average grain size 75μ, are surrounded by a necklace of fine recrystallized grains about 4μ in size. Intermediate sized γ' precipitates (size 0.5μ) are uniformly distributed in the warm worked grains, giving a dark shade to these grains. MC carbides, high in Ti, Nb and W are also randomly scattered through the material. Details of the necklace region are revealed in the scanning micrograph of Fig. 5. The grain boundaries of recrystallized necklace regions are decorated with large γ' (size 1μ). These are apparently larger than those inside the warm worked grains on the adjacent sides because of the partial solutioning. The white particles at the boundaries between the warm worked grain and the necklace region, are the MC carbides which are in relief after electroetching. Fig. 6 shows a transmission micrograph of the necklace region. The fine γ' (size 0.05μ), appearing as small light areas in the background, are, in fact, distributed evenly throughout the material. The recrystallized fine grains are seen to be free of dislocations. Many of them were

twinned as shown in Fig. 7. Here, a warm worked grain is on the left while the necklace region is on the right surrounding it. In the warm worked grain, the residual dislocation substructure introduced during the final forging is clearly evident. The intermediate sized γ', providing a barrier to impede recrystallization or realignment of dislocations into polygonal cells, serves to stabilize the structure.

4.1.2   Low Cycle Fatigue Test Results:

The stress behavior of Rene' 95 during fatigue testing is available in the technical report AFWAL-TR-80-4075. For continuous cycling under total strain control, initially for a short period of time, it exhibited strain hardening. This was followed by strain softening for the rest of the life. In hold time tests, stress usually relaxed rapidly to 80-90 percent of the maximum stress in the first fifteen seconds (see Table III) but remained almost constant thereafter. Non-zero mean stresses[85] were noticable, especially in tests at the lower strain ranges and with longer hold times. In the case of tensile hold tests the maximum tensile stress decreased with cycles while the maximum compressive stress increased, i.e., the hysteresis loop shifted in compressive direction. As a result, the mean stress continued to shift in the compressive direction throughout the life. Shifts to a tensile mean stress occurred for tests under compressive hold but they were less dramatic.

The results of LCF tests on Rene' 95 tested under continuous cycling and with strain holds at 650°C are summarized in Table III. All the stress and strain data listed were values at half life. Note

that the elastic component was much greater than the plastic one. This, in fact, is a common phenomenon in nickel-base superalloys in the strain range of general studies. The mean stress effects cited above are demonstrated in this Table by the differences between maximum tensile and compressive stresses.

Coffin-Manson diagram is shown in Fig. 8. On the basis of plastic strain range, tensile hold and continuous cycling, in general, appeared to exhibit longer life than compressive and balanced (both tensile and compressive) holds. Although differences in life did exist between different cycle types, they did not seem to be very significant. The trend in the large shift mentioned earlier, of the maximum tensile stress developed during hold time with respect to continuous cycling, is shown in Fig. 9. At a given plastic strain range, compressive hold developed higher tensile stress than continuous cycling. Tensile and balanced holds had lower values instead. This shift of tensile stress was especially marked for tensile hold at lower strain ranges. The life of tensile hold here, is greater than that of continuous cycling as shown in Fig. 8. This seems to imply that besides the plastic strain range, stress also should be taken into account in determining the fatigue life. This is due to the marked effect of hold time on the maximum tensile stress. This point will be discussed in more detail later.

4.1.3   Metallography:

(i)   Continuous Cycling (20 cpm)

At higher strain ranges multiple crack initiation was

observed. A typical example is shown in Fig. 10. As apparent in Fig. 10(a), there is a transgranular initiation followed by a mixed mode of propagation. Noting that intergranular cracking, in the case of necklace Rene' 95, means fracture path along the grain boundaries in the necklace regions, the grain boundaries on the fracture surface are, in fact, those of small recrystallized grains 4μ in size. At higher magnification, in Fig. 10(b), striations can be seen in the transgranular crack propagation region near the origin. MC carbides are readily observed on the fracture surface. Here, one MC carbide is situated right at the origin, which was probably responsible for initiation of the crack. Two other MC carbides are also seen near the origin, but apparently had been cut through during crack propagation. This was the case in most other crack initiation regions. Fig. 11 shows another crack initiation region. Here, the crack probably had initiated intergranularly but followed by predominantly transgranular propagation. The striations are clearly visible on the fracture surface and are very brittle in nature. From examination of the longitudinal section, it is seen that majority of the cracks initiated transgranularly. In the case of crack growing more than one grain depth, it often changed directions upon crossing the necklace regions or as it travelled across a single warm worked grain (Fig. 12). Note that the texture of the specimens is such that warm worked grains were elongated in the direction of specimen axis. This, apparently, made the crack path more tortuous. Thus, grain boundary cracking is impeded.

A little away from the initiation region, crack propagation is still by a mixed mode while faceting was frequently found in the warm worked grains (Fig. 13). Menon and Reimann[50,71] have reported earlier, observation of faceting on tensile and fatigue fracture surface of necklace Rene' 95. They speculated it to be due to the microtwinning in the warm worked grains. Oblak and Owczarski[69] have also previously reported, faceting on tensile fracture surface of thermomechanically processed Udimet 700, but they ascribed it to a possible path of failure along (111) slip planes. More recently, Mills[86] observed facets on the fracture surface of Inconel X-750 following tensile deformation. From examination of the longitudinal section, it appeared to have failed along well-defined slip traces. Therefore, he believed that the facets were a result of separation along dislocation channels which, in fact, are slip bands formed by an extensive planar slip of dislocations. For the case of necklace Rene' 95, Mills' reasoning seems to be more applicable. This point will be discussed later in the section on deformed microstructure.

At lower strain ranges, just as at high strain ranges, cracks often initiated at surface connected MC carbides, as shown in Fig. 14. Initial crack propagation appeared to take place transgranularly in the warm worked grains. Whenever it encountered the necklace region, the crack changed its path to follow the grain boundaries. This dual mode of cracking seems to be more extensive and distinct with decreasing strain range. Fig. 15 shows the region of crack initiation and initial propagation of a specimen tested at 0.9 percent

total strain range. The warm worked grains were clearly delineated by the necklace surrounding them. In the warm worked grain where the crack initiated, the crack surface appeared to be very smooth such that even slip traces can be seen on the fracture surface. Although the grain did show slip band formation, there was no evidence to suggest that initiation was due to cracking along slip bands. Rather, a surface-connected MC carbide situated at the origin clearly suggests that the crack had initiated at MC carbide but not along slip band. Following the dual mode of cracking was the normal mixed mode which included those features like striations and facets in the warm worked grains.

In a previous study[73] on crack initiation in necklace Rene' 95 at room temperature, it was found that cracking of MC carbides seemed to play a significant role. In this study also, cracking of MC carbides was seen quite often on the gage surfaces of all the specimens examined. An example is shown in Fig. 16(a), depicting cracking of surface carbides. Fig. 16(b) shows two cracks which had originated from cracking of MC carbides and further propagated into the matrix. Thus, it can be concluded that crack initiation was due to cracking of the surface MC carbides, as those present in the crack initiation region on the fracture surface.

Some of the MC carbides had fractured inside the specimen during deformation (Fig. 17). In specimens tested at higher strain ranges, internal cracks were occasionally seen (Fig. 18). Since the crack did not follow the path of grain boundaries, it could not possibly be due to the effect of creep. It is likely that the crack

had initiated at an internal MC carbide and further propagated transgranularly.

On the gage surface of the specimens slip offsets were sometimes observed (Fig. 19). However, no crack was found to initiate along these slip bands. Occasionally the edges of the fracture surfaces were seen to be parallel to the slip offsets in the crack propagation region (Fig. 20). This, along with the facets found on the fracture surfaces indicate that slip band cracking did play a role in crack propagation. In view of the fractography it seems possible that extensive slip took place only near crbides and eventually crack initiation occurred in slip bands which contained carbides.

(ii) Deformed Microstructure:

Although the TEM study was somewhat limited, some features which are typical and representative were observed in the deformed microstructure. In the warm worked grains, besides a general increase in dislocation density, microtwins and slip bands were also present[87] as shown in Fig. 21. Menon and Reimann[50,71] have reported that the dislocation substructures retained in the warm worked grains was very effective in dispersing slip. This in turn, prevented early formation of intense slip bands and forced the deformation to take place more homogeneously, as compared to the coarse planar slip that occurs in conventional superalloys. This reduced planarity of slip is also illustrated in Fig. 21. Here, slip bands (parallel to (111) planes) are closely spaced and often end at the interior of the grain rather than being wide spaced and crossing the entire grain.The regions

between slip bands also had a high denisty of dislocations, thus obscurring the prominence of the slip bands.

In the last section, a question was raised as to whether the facets observed on the frature surfaces were due to microtwinning or a result of planar slip in the warm worked grains. It was shown that the width of microtwins in Fig. 21 was much smaller than the height of facet steps shown in Fig. 13. Therefore, the facets cannot possibly be a result of microtwinning. Rather, it is believed that with increasing cycles the slip bands which were not intense in the beginning tend to become more intense. This is true especially in those ahead of the crack tips. Therefore, cracking along slip bands (facets) was always seen in the regions of crack propagation.

The deformation in the necklace grains was planar which was also relatively homogeneous in that the interspacing between slip bands was very small (Fig. 22).

(iii) Effect of Hold Time:

When hold time was introduced into each cycle (irrespective of the nature of the hold), fractography revealed an intergranular crack initiation and early crack propagation except at lower strain ranges. Fig. 23 illustrates this intergranular cracking in specimens tested at 1.4 percent total strain range under tensile, compressive and balanced holds respectively. A mixed mode of cracking was again observed away from the origin with occasional facets and striations, as shown in Fig. 24, in the warm worked grains. On the longitudinal section, as shown in Fig. 25, most of the secondary cracks seen were

initiated in the necklace regions (grain boundaries). Fig. 26 shows a crack which although was initiated transgranularly, propagated predominantly along the necklace regions before meeting a warm worked grain. Due to the tortuosity of the grain boundaries, a pure intergranular cracking was hardly seen.

At lower strain ranges, the initiation of cracks again appeared to be associated with MC carbide cracking. The dual mode of cracking, i.e. transgranular in the warm worked grains and intergranular in the necklace grains, was again observed in all types of holds. It was particularly marked in tensile hold, as shown in Fig. 27.

At the interior of the specimens, the damage was not pronounced, indicating that creep did not play an important role in the damage process of hold time tests. Considering the tendency for the crack to initiate intergranularly on the surfaces with the introduction of hold time, a possible involvement of environment appears to be implied. In Fig. 8 it was already shown that tensile hold resulted in life not less than that in continuous cycling. This, then, suggests that the cracking mode (initiation and early propagation) became intergranular under tensile hold in contrast to transgranular mode under continuous cycling. However, the life did not decrease correspondingly. It is clear that in the case of necklace Rene' 95, a decrease in life is not necessarily associated with intergranular cracking. The most likely reason for this is the role of tortuous morphology of grain boundaries mentioned earlier, in slowing down the fracture process when the crack path follows grain boundaries.

As shown in Fig. 8 at a given plastic strain range the differences in fatigue life between different cycle types became substantial at lower strain ranges. However, the mode of cracking still appeared to be very similar to that seen above. This then, implies that differences in fatigue life in this case resulted probably from the different crack propagation rates between the various cycle types.

Recently Coffin[88] has described the importance of mean stress effects in terms of the transition fatigue life, i.e. the life where the elastic and plastic strains are equal. **There the life** exceeds the transition fatigue life, the greater the mean stress effect. The transition fatigue life for Rene' 95 at 650°C has been determined to be about 72 cycles.[89] Consequently, all the tests in this study were conducted above the transition fatigue life. Hence, consequences of the maximum tensile stress (or mean stess) should be considered. This is particularly important when considering the fatigue life controlled by crack propagation, assuming that microcracks have nucleated early in life. Although the plastic strain range remains the same for different cycle type tests, the maximum tensile stress can, indeed, influence the local plastic strain at the crack tip. Higher the maximum tensile stress, greater is the crack opening and faster is the crack growth. This may be the case in Rene' 95, since cracks often initiated at MC carbides.

Previously, in the case of LCF hold time behavior of Cast Rene' 80 at a plastic strain range of 0.32 percent, Lord and Coffin[62] have already demonstrated that mean stress effects could

account for the life behavior in a qualitative sense. The same conclusion can also be drawn in this study. Further, a quantitative dependence of life on maximum tensile stress is shown in Fig. 28. The data seem to fall generally onto three lines, corresponding to the three respective tensile hold times - 0, 1 and 10 minutes. The observed behavior not only illustrates the important role of the maximum tensile stress in determining the fatigue life, but also demonstrates the influence of tensile hold time on fatigue life. Whether this behavior has any mechanistic basis is not known at the present time. However, it tends to imply that crack growth is promoted by introduction of a tensile hold.

Previously Wright and Anderson[90] found that in directionally solidified Rene' 120, under strain controlled testing, the developed stress levels and the lives varied with orientation. This was because of the dependence of the elastic modulus on orientation. Consequently, they found that most of their LCF data for various orientations fit one master curve, when the maximum tensile stress rather than total strain range was plotted against life. Considering LCF as mainly a process of crack growth the authors recommended using maximum tensile stress as a life prediction parameter.

In this study, due to the effect of the two variables, plastic strain range and maximum tensile stress, comparison of the lives between cycle types became difficult. On the basis of maximum tensile stress alone, life seems to depend only on tensile hold time. Therefore, quite contrary to the result shown in Fig. 8, simply on the

basis of plastic strain range, life of tensile hold is comparable to that of continuous cycling but greater than that of compressive hold. Although the relative contribution of these two variables in determining the fatigue life is not clear, however, the effect of maximum tensile stress is distinct and has to be taken into account in any life prediction scheme.

4.1.4   Applicability of Fatigue Model:

With the experimental data in this study for necklace Rene' 95 at 650°C, four fatigue life models were evaluated earlier.[89] Their applicability and limitations in predicting lives corresponding to various cycle types are summarized in Table IV. The established criterion for accepting predicted lives was that predicted lives should be within a factor of two of the observed lives. If the predicted values were greater than twice the observed lives, the model was considered to overpredict. By the same token, when it was less than half the observed lives, the model was regarded as underpredicting the lives.

In general, all the models showed a tendency to underpredict lives of tensil hold, Also, in the case of compressive hold, with the exception FS model, they all resulted in overprediction. As mentioned earlier under tensile hold the creep effects (internal damage) in Rene' 95 were almost absent. But,

because of the comparatively lower maximum tensile stress, life of tensile hold was greater than that of compressive hold. Thus, underprediction of the lives by these two models for tensile hold and overpredition for compressive hold is understandable.

In applying Ostergren's model, the time-dependent, wave shape independent situation was considered, where $\nu = 1/(\tau_o + \tau_T + \tau_c)$ (cyclic frequency). Even though in this life prediction scheme, maximum tensile stress was incorporated into the damage term, prediction of lives at lower strain ranges and under longer hold times was difficult. It should be noted that at lower strain ranges higher degree of scatter in the data is always present in part due to the uncertainty in the experimental procedures. This uncertainty in turn makes accurate life predictions more difficult. From this study, it is recognized that both plastic strain range and maximum tensile stress can be the variables controlling the fatigue life. Interaction between these two in relation to the different cycle types is not adequately understood at the present time. Further, the time dependent factor in determining life seems to be the tensile hold time rather than the cycle period (reciprocal of cyclic frequency) used in Ostergren's model. Thus, question still remains as to the validity of the damage term employed in the Ostergren's model.

Overall, the LCF behavior of nickel-base superalloy Rene' 95 was seen to be quite different from that of stainless steel. However, it was similar to that of Rene' 80[62] with no pronounced creep effect under tensile hold. The life prediction models that associate creep

with tensile hold were rendered inapplicable. Due to the limited information available in this study, no attempt was made to develop a suitable life model to describe the LCF behavior of Rene' 95. It is believed that any life prediction scheme, in order to be applicable, should incorporate the fact that tensile hold promotes crack propagation and the effect of maximum tensile stress. Before attempting to develop any model, more work needs to be done in estimating the relative proportion of life corresponding to crack initiation and propagation as well as the possible involvement of environment, which was reported in creep for Cast + Forged Rene' 95[73] and in fatigue for HIP + Forged Rene' 95[9], with respect to different cycle types.

4.2   NARloy Z:

4.2.1   Initial Structure:

The initial structure of NARloy Z is shown by the optical micrographs in Fig. 29. The average grain size was determined as 150μ (ASTM No. 3) by linear intercept method. The intermetallic compound resulting from the addition of Zr to the Cu-Ag entectic system is visualized and has been identified as Cu-10Ag-22.5 Zr with a tetragonal structure.[74] Two types of precipitates in the Cu rich matrix are shown in Fig. 30(a) transmission micrograph. One of these is larger, and tends to grow on certain crystallographic planes, the other relatively small and evenly distributed in the background. Analyzing the diffraction pattern shown in Fig. 30(b) using the selected area diffraction technique, the former is identified as Ag which gives rise to rings and the latter, Cu_2O (cuprous oxide) which gives rise to

superlattice spots. Ag precipitates, having FCC structure, normally are found in the form of plates, lying parallel to (111) or (100) planes of the Cu matrix with random directions.[91] This is the reason why rings, corresponding to Ag, are present in Fig. 30(b) under (111) diffraction. Cu_2O precipitates, having C3 cubic structure,[91] exhibit orientation same as the Cu matrix. The slightly different lattice parameters make both precipitates semi-coherent. Rockwell International Inc., who developed this material did not report the presence of Cu_2O which is probably a result of internal oxidation.

4.2.2   Low Cycle Fatigue Test Results:

Table V summarizes the results of LCF tests at 538°C under continuous cycling and with strain holds. The higher ductility and low strength of NARloy Z is reflected by the plastic component much greater than the elastic one. The life, therefore, was dominated by the former and was truly in the LCF regime. For continuous cycling tests, stress range was very sensitive to strain rate especially in the high strain range. For hold time tests maximum tensile stress was only dependent on the strain range and almost independent of the cycle character. Stress relaxation during hold time was very pronounced in NARloy Z. This is indicative of significant creep and/or creep crack growth, i.e. the creep effect may have played an important role in the damage process. The Coffin-Manson diagram is shown in Fig. 31. Apparently cyclic life decreased with decreasing strain rate under continuous cycling. Further, tensile hold was the most detrimental among the cycle types in interest. Life in the case of compressive

hold was comparable with that of continuous cycling at high strain rate of 1.0 percent sec^{-1}. It is worthwhile noting that the difference in lives between cycle characters are much greater in NARloy Z than in Rene' 95.

4.2.3   Metallography:

(i)   Effect of Frequency:

In specimens tested at high strain rate, integranular surface cracks had initiated and grown two or three grains in depth by a boundary mechanism before changing to transgranular. Such a transition from intergranular to transgranular is shown in Fig. 32(a). The striations are clearly seen in the region of transgranular crack propagation (Fig. 32(b)). No significant differences were seen in fracture details between high strain range (2.6 percent) and low strain range (0.9 percent) tests. They both had a multiple crack origins and final rupture of the specimens took place in the center of the overload region. A number of grain boundaries on the gage surface had undergone decohesion. As shown in Fig. 33, cracking of some of these were connected with the fracture surface. From examination of the longitudinal section, it is seen that most of these intergranular surface cracks either had ceased growing right after initiation as in Fig. 34(a) or had grown two or three grains in depth (Fig. 34(b)). The fact that boundary cracking is limited to regions near the surface seems to imply that it is was probably either environmentally assisted or due to a creep effect (where the grains are unconstrained and sliding is easier). The role of environment will be discussed in

greater detail later. Fig. 34(c) shows an intergranular surface crack which had propagated like the main crack, transgranularly into the matrix.

Away from the surface, intergranular damage in the form of wedge type cracking (Fig. 35(a)) and cavitation (Fig. 35(b)) was observed at high strain range. However, considering the fact that the main crack propagated by a transgranular mode, such damage does not seem to play an important role as far as crack propagation is concerned.

As the strain rate decreased, cracking became predominantly intergranular and striations were absent from the fracture surface, as shown in Fig. 36. Extensive grain boundary cracking on the gage surface (Fig. 37) was again observed in low strain rate tests. Discoloration of the specimens and obscuring of the fracture details in Fig. 36 indicate that oxidation had occurred during testing. The oxidation is probably due to the reaction of the trace of oxygen and/or moisture in the Argon environment. Thus even though the environment was supposed to be inert, in reality, environmental contamination was still present. As seen in Fig. 37, preferential grain boundary oxidation is more pronounced in this case than in high strain rate tests (Fig. 33). Meanwhile, on the longitudinal section the surface cracks seemed to have grown deeper into the matrix (Fig. 38), as compared to cracks in the case of high stain rate. These phenomena occur because of the longer exposure of the specimens to the environment (longer duration of testing) tested at low strain rate. Internal

intergranular damage, though it was again observed at low strain rate, was not extensive (Fig. 39). This raises the question whether the intergranular fracture in low strain rate tests was a result of the link-up of internal cracks or due to the effect of environment. Evidence of oxidation on the entire fracture surface suggests the involvement of environment. However internal cracking is unaffected by environment. The presence of longer surface cracks (Fig. 38) and the fact that specimens failed at the center indicate that fracture is a result of propagation of surface cracks along grain boundaries radially toward the center before final rupture. The same observations were made from specimens tested at low strain range except that internal damage was absent. Failure path for the low strain rate tests indicates that intergranular fracture was probably due to the environmental effects rather than the link-up of internal cracks. Coffin[76] also observed intergranular cracking in OFHC copper tested at a strain rate of 0.0033 percent sec^{-1} in air and attributed it to environment-controlled fatigue.

Metallography of the specimens indicated that the decrease in cyclic fatigue life with decreasing strain rated was associated with a change in fracture from transgranular to intergranular cracking. Such frequency dependence of fatigue life and type of fracture is attributed to a greater environmental involvement with decrease in frequency. This is consistent with the previous

observation and conclusion made by Gell and Duquette in A286 tested in air.[40] It is generally believed that oxidation promotes surface intergranular initiation and propagation along the grain boundaries which are the easiest diffusion paths for oxygen. The degree to which the fracture is intergranular, then, depends on the material, frequency and strain rate.

(ii) Effect of Hold Time:

As indicated in Table V the cyclic lives were comparable for both compressive hold and continuous cycling at high strain rate. This fact is also borne out by fractography. Fig. 40 shows the transition of cracking from intergranular to transgranular under compressive hold, as previously seen in Fig. 32(a) Striations can be seen at higher maginfication but are obscured by estensive surface oxidation. Preferential grain boundary oxidation on the side surface was severe, especially in the specimen tested at low strain range (Fig. 41). These specimens had the longest life time among the specimens examined. Internal and surface cracks were both present, with no difference from continuously cycled material. A unique feature noted in the specimen tested at low strain range was the evidence of recrystallization in the gage section, as shown in Fig. 42. A similar observation was made by Pavinich and Raj[22] in Cu-Si alloy under constant load at 800°C, and in vacuum - cast copper under fatigue at 500°C by Wigmore and Smith.[75] This phenomenon is, apparently, a result of dynamic recrystallation which occurred during the long duration of testing the specimen was subjected to.

Under tension hold, cracking was predominantly intergranular (Fig. 43). The dimples, resulting from final overload rupture, were distributed uniformly rather than being concentrated in the center. Intergranular cracks observed at the interior in this case (Fig. 44) seem to be much longer than those seen previously. This is due to the interlinkage of several cracks. Internal damage was seen in specimens tested at both high (Fig. 44) and low strain ranges, as illustrated in Fig. 45. Notice that in Fig. 45 an internal crack is linked up with a surface crack. In this case failure is due to the link-up of internal intergranular cracks and concurrent intergranular propagation of cracks initiated externally. The relative importance of the internal and external cracks is not known at present.

Tensile hold is more damaging than compressive hold for NARloy Z, as in stainless steel.[31-33] Fracture in the former case is intergranular mainly due to creep and environmental effects, while it is transgranular in the latter case, similar to that in continuous cycling at high strain rate.

4.2.4   Damage Mechanisms:

From the metallographic results it is clear that in NARloy Z three types of damage occur during fatigue associated with the effects of creep, environment and cyclic strain. For all the cycle characters of interest, cracks always initiate at grain boundaries due to either the effect of environment or creep effect. The fatigue life was, therefore, controlled by the fastest damage mechanisms that are

operating under the test conditions. For continuous cycling at high strain rate, creep and environmental effects are very minor. Therefore, cracking is transgranular resulting from cyclic strains. As strain rate decreases, both creep and environmental effects become important. Intergranular cavitations and triple point cracks though formed during the tensile half cycle are substantially re-welded during the compressive half cycle by slowly reversed grain boundary sliding. This reversal of creep damage renders the environmental effect a dominant source of damage. The interaction of the hostile environment with the cracks during tensile half cycle leads to intergranular fracture. In the case of compressive hold, the tensile going strain rate is still high such that both creep and environmental effects are insignificant. therefore, a normal transgranular fatigue crack results. On the other hand, in the case of tensile hold both creep and environment effects should be considered. The internal damage (cavities or wedge cracks) produced during the hold time can hardly be re-welded due to the high compressive-going rate. As a result, linkup of cracks takes place at the interior. Concurrently, during tensile hold time environmental attack takes place, resulting in intergranular cracking starting from the surface. The rate of combination of these two processes is faster than that of the external damage from the environment alone. Eventually fracture is intergranular mainly due to both creep and environmental effects.

Thus, each damage mechanism seems to be favored under certain test conditions. Creep effects dominate in the case of tests

with slow tensile-going rate or tensile hold time but fast compressive-going rate. Slow tensile-going rate, regardless of compressive strain rate, favors environmental damage. Cyclic strain damage becomes most important when the tensile-going rate is fast. For NARloy Z in terms of cyclic life (Fig. 31), creep is most damaging, followed by environmental effect, while cyclic strain is relatively the least harmful.

More data from continuous cycling and unequal strain rate tests are shown in Fig. 46 with the data from Fig. 31 superimposed. Note that for continuous cycling at three different strain rates, life decreases with decreasing strain rate. This illustrates that environmental effect is time dependent in general. In unequal strain rate tests, slow-fast tests are more damaging than fast-slow tests, as implied in the above discussion. In slow-fast tests life decreased with decreasing tensile-going rate. This illustrates the time dependence of creep process. A qualitative damage picture with respect to the test conditions is summarized in Table VI.

4.2.5   Deformed Microstructure:

Transmission electron microscopic analysis of LCF tested microstructure was done on selected specimens. In specimens tested at low strain range at the low rate of cycling and with tensile hold, a varied substructure was seen in different grains. Fig. 47(a) shows a random distribution of dislocations in one grain with a low dislocation. Most of these were pinned by Ag precipitates which had coarsened during testing. In the same specimen subgrains had also formed in

some grains (Fig. 47(b)). The variation of substructure has been observed earlier in austenic stainless steel under tensile[92] and fatigue deformation.[93] It is mainly due to the difference in orientations of the grains with respect to the stress axis, which results in different shear stresses on the active slip planes in different grains. Fig. 47(a) represents a grain which was less favorably oriented to the stress axis. Low shear stress on the active slip planes did not enable dislocation to overcome the precipitate barriers, except by thermally activated cross-slip and/or climb. In the case shown in Fig. 47(b) the grain was favorably oriented and shear stress was sufficiently high to let dislocations overcome the precipitates by looping along with cross-slip and/or climb. Eventually dislocations rearranged themselves into a low energy configuration like subgrain boundaries. Both stress and time are expected to be two main factors in determining the detailed deformed substructure, e.g., the former may control the subgrain size,[93] while the latter can promote cross-slip and may influence the relative orientations between the subgrains.[94] The occurrence of recrystallization under compressive hold at low strain range is apparently an extreme case representing the time effect. More TEM study needs to be done to completely characterize the deformed microstructure of NARloy Z with respect to stress (strain) and time.

4.2.6   Applicability of Fatigue Life Models:

In view of the limited data available for each cycle type, an evaluation of each model for its life prediction capability was not

included in the scope of this study. However, according to their inherent assumptions in relation to the damage mechanisms discussed in the previous section, an attempt will be made to suggest the possible applicability of them to certain cycle characters for NARloy Z.

It has been shown that in NARloy Z, each cycle character has specific damage mechanisms associated with it, e.g., cyclic strain with continuous cycling at high strain rate (pp cycle) and compressive hold (pc cycle), environmental effect in the case of continuous cycling at low strain rate (cc cycle) and both creep and environmental effects with tensile hold (cp cycle). Earlier, it has been mentioned that the fatigue life is indeed determined by the plastic strain component in NARloy Z. Therefore, the conventional Coffin-Manson law is, apparently, applicable to pp and pc cycles where the life is cycle-dependent rather than time-dependent and damage is due to cyclic strain only. In the case of cc cycle, Coffin's frequency modified model, which incorporates the time-dependent factor to account for the sensitivity of crack growth rate and mode of cracking to the environment,[88] appears to be more applicable. As far as cp cycle is concerned, the case seems to be more complicated. Even though environmental and creep effects are two apparent damage modes, the possible physical interaction between them cannot be ruled out. For example, oxidation along the grain boundary during the tensile half cycle may inhibit the re-welding of the voids during the compressive half cycle. This, in turn, promotes internal damage. Among the life prediction methodologies, none of them appears to incorporate the

possible interaction between these two damage modes. Thus, it is difficult to make relevent suggestions as to the model applicable in pc cycle.

In summary, instead of evaluation of each model for all cycle characters, suggestions have been made as to the possible applicability of a certain model to a certain cycle character in terms of damage mode (Table VI). As far as the adequacy of the damage terms employed in these models to describe the corresponding damage mechanisms is concerned, in view of the limited data available (two for most cycle types) the author has no comments at this stage. It should be realized that the development of a life prediction scheme for a particular system is more complicated than the actual way most of the existing models were developed. Basically, it involves procedures as follows:

(i)   identify the damage mechanisms

(ii)   identify the variables that affect the mechanisms
        (i), e.g., plastic strain, maximum stress, mean
        stress, frequency, hold time, strain rate, etc.

(iii)   quantify (i) as functions of (ii).

(iv)   identify critical damage tolerance.

(v)   formulate fatigue life by combining (iii) and (iv).

5. SUMMARY AND CONCLUSIONS

Damage mechanisms were studied in two candidate materials for aerospace applications. They are the nickel-base superalloy Rene'95 and copper base alloy NARloy Z, exhibiting quite different microstructures, strengths and ductilities. All the specimens examined in this study were already tested earlier for the AGARD SRP program. Continuous cycling and hold time tests were performed at 650°C for Rene '95 and at 538°C for NARloy Z. Optical, scanning and transmission electron microscopy were used to determine the deformation mode and fracture characteristics. The important conclusions derived from this investigation are:

1. In the case of Rene '95, planar slip and microtwinning are the two modes of deformation, while dispersive slip is the mode of deformation in NARloy Z.

2. The elongated warm worked grains in Rene '95 result in the tortuosity of the grain boundary morphology, which in turn acts to impede intergrannular cracking.

3. Within the total strain ranges of interest, fatigue life is dominated by plastic strain range in NARloy Z, representing a material of low strength and high ductility, while it is elastic strain range in the case of Rene '95, representing a material of high strength and low ductility.

4.   Crack initiation in Rene '95 under continuous cycling is
        mainly due to a cracking of surface MC carbides. A mixed
        mode of propagation with a faceted fracture morphology is
        observed at high strain ranges. At lower strain ranges, a
        dual mode - transgranular in worked grains and intergranu-
        lar in necklace regions - is typical.

5.   In hold time tests for Rene '95, at high strain ranges,
        regardless of the nature of hold, cracks initiate predomi-
        nantly at grain boundaries and propagate by a mixed mode.
        At low strain ranges, however, crack initiation is asso-
        ciated with MC carbide cracking and initial propagation is
        by the dual mode.

6.   In Rene '95 at a given plastic strain range, compressive
        hold appears more detrimental mainly due to a higher maxi-
        mum tensile stress produced. The dependence of fatigue
        life on maximum tensile stress is demonstrated by the data
        falling onto three separate lines corresponding to the
        three tensile hold times, in the life against maximum ten-
        sile stress plot.

7.   In NARloy Z, under continuous cycling crack initiation at
        grain boundaries is due to environmental and/or creep
        effects. As strain rate decreases the mode of crack pro-
        pagation changes from transgranular to intergranular

because of greater environmental involvement resulting in a decrease in life.

8.   At a given plastic strain range, tensile hold is more detrimental than compressive hold in NARloy Z. Life of compressive hold is comparable with that of continuous cycling at high strain rate and so is the fractography. Intergranular cracking in the case of tensile hold, which results from the concurrent effects of creep (irreversible internal damage) and environment, makes it most detrimental among the cycle characters of interest.

9.   A basic requirement for a life prediction scheme to to be applicable to Rene' 95 is incorporation of the effect of maximum tensile stress, and the fact that tensile hold promotes crack propagation.

10.   In the case of NARloy Z, a life prediction model based on observed damage mechanisms is needed.

REFERENCES

1. Manson, S.S., Halford, G.R. and Hirschberg, M.H., "Creep-Fatigue Analysis by Strain Range Partitioning", NASA TM X-67838, 1971.

2. Coffin, L.F. "The Concept of Frequency Separation in Life Prediction for Time-Dependent Fatigue", ASME MPC Symposium on Creep-Fatigue Interaction, ASME MPC-3, 1976, pp. 349.

3. Ostergren, W.J., "A Damage Function and Associated Failure Equations for Predicting Hold Time and Frequency Effects in Elevated Temperature, Low Cycle Fatigue", J. of Testing and Evaluation, 4 (5), 1976, pp. 327.

4. Majumdar, S. and Maiya, P.S. "A Unified and Mechanistic Approach to Creep Fatigue Damage", ANL-76-58, 1976.

5. Gell, M. and Leverant, G.R., Fatigue at Elevated Temperatures, ASTM STP-520, 1973, pp. 37.

6. Antolovich, S.D. "La Fatigue des Materiaux et des Structures" Ed. Bathias, C., Balion, J.P. and Maloin, S.A., Paris, 1980, pp. 465.

7. Wells, C.H., Sullivan, C.P. and Gell, M., "Mechanisms of Fatigue in the Creep Range", Metal Fatigue Damage, ASTM STP 495, 1971, pp. 61.

8. Grosskreutz, J.C., Metal Fatigue Damage, ASTM STP 495, 1971, pp. 5.

9. Bashir, S., Taupin, Ph. and Antolovich, S.D., "Low Cycle Fatigue of As-HIP and HIP + Forged Rene' 95", Met. Trans., 10A, 1979, pp. 1481.

10. Coffin, L.F., Proc. of the Third Conf. on Fracture, Munich, April 8-13, 1973, pp. V-441/A.1.

11. Gell, M. and Leverant, G.R., "The Effect of Temperature on Fatigue Fracture in a Directionally Solidified Nickel-Base Superalloy", Proc. of the Second International Conf. on Fracture, 1969, pp. 565.

12. Leverant, G.R. and Gell, M., "The Elevated Temperature Fatigue of a Nickel-Base Superalloy, Mar-M200, in Conventionally-Cast and Directionally-Solidified Forms", Trans. Metallurgical Society, American Institute of Mining, Metallurgical, and Petroleum Engineers, 245, 1969, pp. 1167.

13. Wells, C.H. and Sullivan, C.P., "Low-Cycle Fatigue Dmage of Udimet 700 at 1400°F", ASM Trans. Quarterly, 158, 1965, pp. 391.

14. Campbell, L., "The Influence of Metallurgical Structure on the Mechanisms of Fatigue Crack Propagation", Fatigue Crack Propagation, ASTM STP 415, 1967, pp. 131.

15. Saxena, A. and Antolovich, S.D., "Low Cycle Fatigue Crack Propagation and Substructures in a Series of Polycrystalline Cu-Al Alloys", Met. Trans., 6A, 1975, pp. 1809.

16. Veevers, K. and Snowder, K., "High-Temperature Intercrystalline Fatigue Failure: A Review", J. of the Australian Institute of Metals, 20, 1975, pp. 201.

17. McLean, D. and Farmer, M.H., "The Relation dueing Creep between Grain-Boundary Sliding, Sub-Crystal Size, and Extension", J. of the Institute of Metals, 85, 1956, pp. 41.

18. Mellendore, A.W. and Grant, N.J., "Grain Boundary Sliding During Creep of an Al-2% Mg Alloy", Trans. Metallurgical Society, American Institute of Mining, Metallurgical and Petroleum Engineers, 227, 1963, p. 319.

19. Williams, H.D. and Corti, C.W., "Grain-Boundary Migration and Cavitation During Fatigue", Met. Sci. J., 2, 1968, pp. 28.

20. Gittins, A., "The Effect of Long-Range Order on the High Temperature Fatigue Behavior of Cu_3Au", Met. Sci. J., 2, 1968, pp. 114.

21. Skelton, R.P., "The Growth of Grain Boundary Cavities During HIgh Temperature Fatigue", Phil. Mag., 14, 1966, pp. 563.

22. Pavinich, W. and Raj, R., "Fracture at Elevated Temperature", Met. Trans. 8A, 1977, pp. 1917.

23. Williams, H.D., "Fractographic Observations of High-Temperature Fatigue Cavitation", Acta Met., 16, 1968, pp.771.

24. Leverant, G.R. and Sullivan, C.P., "The Low-Cycle Fatigue of TD-Nickel at 1800°F", Trans. Metallurgical Society, American Institute of Mining, Metallurgical, and Petroleum Engineers, 245, 1969, pp. 2035.

25. Runkle, J.C. and Pelloux, R.M., Micromechanisms of Low-Cycle Fatigue in Nickel-Based Superalloys at Elevated Temperatures", Fatigue Mechanism, ASTM STP 675, 1979, pp. 501.

26. Merrick, H.T., "The Low Cycle Fatigue of Three Wrought Nickel-Base Alloys", Met. Trans., 5, 1974, pp. 891.

27. Wells, C.H. and Sullivan, C.P., "Interactions between Creep and Low-Cycle Fatigue in Udimet 700 at 1400°F", Fatigue at High Temperature, ASTM STP 459, 1969, pp. 59.

28. May, M.J. and Honeycombe, R.W.K., "The Effect of Temperature on the Fatigue Behavior of Mg and Some Mg Alloys", J. of Institute of Metals, 92, 1863-64, pp. 41.

29. Gittins, A., "The Effect of Long-Range Order on the High-Temperature Fatigue Behavior of Cu_3Au", Met. Sci. J., 2, 1968, pp. 114.

30. Stroh, A.N., "The Formation of Cracks as a Result of Plastic Flow", The Royal Society, Series A, 223, 1956, pp. 404.

31. Berling, J.T. and Conway, J.B., Hold Time Effects in High Temperature Low-Cycle Fatigue, ASTM STP 489, 1971, pp. 12.

32. Majumdar, S. and Maiya, P.S., "Inelastic Behavior of Pressure Vessel and Piping Components", PVP-PB-028, 1978, pp. 43.

33. Manson, S.S., "The Challenge to Unify Treatment of High Temperature Fatigue", Fatigue at Elevated Temperatures, ASTM STP 520, pp. 744.

34. Coffin, L.F., "Observations and Correlations Emphasizing Frequency and Environmental Effects", Time-Dependent Fatigue of Structural Alloys, ORNL 5073, 1977.

35. Min, B.K. and Raj, R., "A Mechanism of Intergranular Fracture During High-Temperature Fatigue", Fatigue Mechanisms, ASTM STP 675, 1979, pp. 569.

36. Coffin, L.F., "The Effect of High Vacuum on the Low Cycle Fatigue Low", Met. Trans. 3, 1972, pp. 1777.

37. Berling, J.T. and Slot, T., "Effect of Temperature and Strain Rate on Low-Cycle Fatigue Resistance of AISI 304, 316 and 348 Stainless Steels", Fatigue at High Temperature, ASTM STP 465, 1968, pp. 3.

38. Coffin, L.F., Proc. of International Conf. on Fatigue: Chemistry, Mechanics and Microstructure, NACE-2, 1972, pp. 590.

39. McMahon, C.J. and Coffin, L.F., Met. Trans. 1, 1970, pp. 3443.

40. Gell, M. and Duquette, D.J., Corrosion Fatigue

41. Paskiet, G.F., Boone, D.H. and Sullivan, C.P., J. of the Institute of Metals, 100, 1972, pp. 58.

42. Duquette, D.J. and Gell, M., "The Effects of Environment on the Elevated Temperature Fatigue Behavior of Nickel-Base Superalloy Single Cyrstal", Met. Trans., 3, 1972, pp. 1899.

43. Organ, F.E. and Gell, M., "Temperature Fatigue of a Nickel-Base Superalloy", Met. Trans, 2, 1971, pp. 943.

44. Aning, K. and Tien, J.K., "Creep and Stress Rupture Behavior of a Wrought Nickel-Base Superalloy in Air and Vacuum", Mater. Sci. and Eng., 43, 1980, pp. 23.

45. Decker, R.F. and Sim, C.T., Ch. 2., The Superalloys, 1972, pp. 33.

46. Stoloff, N.S., ch. 3., The Superalloys, 1972, pp. 79.

47. Wells, C.H. and Sullivan, C.P., "The Effect of Temperature on the Low-Cycle Fatigue Behavior of Udimet 700", Trans. Quarterly, 60, 1967, pp. 217.

48. Moon, D.M. and Sabol, S.P., "Effect of Mean Stress on the HCF Behavior of Udimet 710 at 1000°F", Fatigue at Elevated Temperature, ASTM STP 520, 1972, pp 438.

49. Leverant, G.R. and Gell, M., "The Influence of Temperature and Cyclic Frequency on the Fatigue Fracture of Cube Oriented Nickel-Base Superalloy Single Crystal", Met. Trans., 6A, 1975, pp 367.

50. Menon, M.N. and Reimann, W.H., "Low Cycle Fatigue Crack Initiation Study in Rene' 95", J. of Mater. Sci. and Eng. 10, 1975, pp. 1571.

51. Duquette, D.J. and Gell, M., "The Effect of Environment on the Mechanism of Stage I Fatigue Fracture", Met. Trans, 2, 1971, pp. 1325.

52. Bartos, J. and Antolovich, S.D., "Effect of Grain Size and Size on Fracture Crack Propagation in Rene' 95", Fracture, 2, 1977, pp. 996.

53. Antolovich, S.D., Bathias, C., Lawless, B., Boursier, B., "The Effect of Microstructure on the FCP Properties of Waspaloy", Met. Trans., 1981, pp.

54. Merrick, H.F. and Floreen, S., "The Effect of Microstructure on Elevated Temperature Crack Growth in Ni Base Alloys", Met. Trans., 9A, 1978, pp. 231.

55. Mills, W.J. and James, L.A., "Effect of Heat Treatment on Elevated Temperature Fatigue Crack Growth Behavior of Two Heats of Alloy 718", ASME Publication 7-WA/PUP-3, 1979.

56. Clavel, M., Levaillant, C., Pineau, A., Creep-Fatigue-Environment Interactions, AIME, 1980, pp. 24.

57. Lerch, B., "Effect of Microstructure on the LCF Properties of Waspaloy", M.S. Thesis, University of Cincinnati, 1981.

58. Wells, C.H. and Sullivan, C.P., "Low-Cycle Fatigue of Udimet 700 at 1700°F", Trans. Quarterly, 61, 1968, pp. 149.

59. Coffin, L.F., "The Effect of Frequency on the Cyclic Strain and Fatigue Behavior of Cast Rene' at 1600°F", Met. Trans., 5, 1974, pp. 1053.

60. Antolovich, S.D., Domas, P., Strudel, J.L., "Low-Cycle Fatigue of Rene' 80 as Affected by Prior Exposure", Met. Trans., 10A, 1979, pp. 1859.

61. Floreen, S. and Kane, R.H., "Effects of Environment on High-Temperature Fatigue Crack Growth in a Superalloy", Met. Trans., 10A, 1979, pp. 1745.

62. Lord, D.C. and Coffin, L.F., "Low Cycle Fatigue Hold Time Behavior of Cast Rene' 80", Met. Trans., 4A, 1973, pp. 1647.

63. Teranishi, H. and McEvily, A.J., "The Effect of Oxidation on Hold Time Fatigue Behavior of 2.25 Cr-1 Mo Steel", Met. Trans., 10A, 1979, pp. 1806.

64. Shahinian, P. and Sadananda, K., "Effects of Stress Ration and Hold Time on Fatigue Crack Growth in Alloy 718", ASME Trans., J. of Eng. Mater. and Techn., 101, 1979, pp. 224.

65. Sadananda, K. and Shahinian, P., "Hold-Time Effect on High Temperature Fatigue Crack Growth in Udimet 700", J. of Mater. Sci., 13, 1978, pp. 2347.

66. Sadananda, K. and Shahinian, P., Creep-Fatigue-Environment Interactions, AIME, 1980, pp. 86.

67. Antolovich, S.D., Liu, S. and Baur, R., "Low-Cycle Fatigue Behavior of Rene' 80 at Elevated Temperatures", Met. Trans., 12A, 1981, pp. 473.

68. "Rene' 95 Alloy, Processing and Properties", General Electric.

69. Oblak, J.M. and Owczarski, W.A., "Thermomechanical Strengthening of a γ' Precipitation-Hardened Nickel-Base Alloy", Met. Trans., 3, 1972, pp. 617.

70. Shamblen, C.E., Allen, R.E. and Walker, F.E., "Effect of Processing and Microstructure on Rene' 95", Met. Trans., 6A, 1975, pp. 2073.

71. Menon, M.N. and Reimann, W.H., "Tensile Behavior of Rene' 95 in the Thermomechanically Processed and Conventionally Processed Forms", Met. Trans., 6A, 1975, pp. 1075.

72. Menon, M.N. and Reimann, W.H., "Deformation Twins in Rene' 95", Metallography, 8, 1975, pp. 221.

73. Menon, M.N., "The Effect of Environment on the Creep and Stress Rupture Behavior of Rene' 95", J. of Mater. Sci., 11, 1976, pp. 984.

74. Paton, N.E. and Robertson, W.M., Internal Progress Report, Rockwell International, 1973.

75. Wigmore, G. and Smith, G.C., "The Low-Cycle Fatigue Behavior of Copper at Elevated Temperatures", Met. Sci. J., 5, 1971, pp. 58.

76. Abdel-Raouf, H., Plumtree, A. and Topper, T.H., "Temperature and Strain Rate Dependence of Cyclic Deformation Response and Damage Accumulation in OFHC Copper and 304 Stainless Steel", Met. Trans., 5, 1974, pp. 267.

77. Sidey, D. and Coffin, L.F., "Low Cycle Fatigue Damage Mechanisms at High Temperature", _Fatigue Mechanisms_, ASTM STP 675, 1979 pp. 528.

78. Manson, S.S., Halford, G.R. and Hirschberg, M.H., "Strain Range Partitioning - A Tool for Characterizing High Temperature, Low-Cycle Fatigue", NASA TMS-71691, 1975.

79. Ostergren, W.J., "Correlation of Hold Time Effects in Elevated Temperature Low Cycle Fatigue Using a Frequency Modified Damage Function", _ASME MPC Symposium on Creep-Fatigue Interaction_, ASME MPC-3, 1976, pp. 179.

80. Majumdar, S. and Maiya, P.S., "A Damage Equation for Creep-Fatigue Interaction", _ASME MPC Symposium on Creep-Fatigue Interaction_, ASME MPC-3, 1976, pp. 323.

81. Antolovich, S.D., Baur, R. and Liu, S., "A Mechanistically Based Model for HIgh Temperature LCF of Ni Base Alloys", _Superalloys_, 1980, pp. 605.

82. Hyzak, J.M. and Bernstein, H.L., An Analysis of the Low Cycle Fatigue Behavior of the Superalloy Rene' 95 by Strain Range Partitioning", _Characterization of Low Cycle High Temperature Fatigue by the Strain Range Partitioning Method_, AGARD-cp-243, 1978, pp. 11-1.

83. Stentz, R.H., Berling, J.T. and Conway, J.B., "An Application of Strainrange Partitioning to Copper-Base Alloy at 538°C", AGARD-cp-243, 1978, pp. 12-1.

84. Menon, M.N., "Metallographic Characterization of Rene' 95 Forgings", AFML-TR-73-180, 1973.

85. Manson, S.S., _Thermal Stress and Low-Cycle Fatigue_, 1966, pp. 172.

86. Mills, W.J., "The Deformation and Fracture Characteristics of Inconel X-750 at Room Temperature and Elevated Temperatures", Met. Trans. _11A_, 1980, pp. 1039.

87. Private Communication with Dr. Jude Foulds.

88. Coffin, L.F., "Fatigue at High Temperature-Prediction and Interpretation", Proc. of the Conference on Creep and Fatigue at Elevated Temperature, 1974, pp. 109.

89. Bernstein, H.L., "An Evaluation of Four Current Models to Predict the Creep-Fatigue Interaction in Rene' 95", AFML-TR-79-4075, 1979.

90. Wright, P.K. and Anderson, A.F., "The Influence of Orientation on the Fatigue of Directionally Solidified Superalloys", Superalloys, 1980, pp. 689.

91. Newkirk, J.B., in the Ch. of "Metallographic Principles" Transformation Structures", Metals Handbook, 8, pp. 175.

92. Monteiro, S.N. and Kesterbach, H.J., "Influence of Grain Orientation on the Dislocation Substructure in Austenitic Stainless Steel", Met. Trans., 6, 1975, pp. 938.

93. Ermi, A., "Correlation of Substructure and Crack Behavior with Creep-Fatigue Properties of 304 Stain Steel" Ph.D. Dissertation, University of Cincinnati, 1979.

94. Nahm, H., Moteff, J. and Diercks, D.R., "Substructural Development during Low Cycle Fatigue of AISI 304 Stainless Steel at 649°C", Acta Met. 25, 1977, pp. 107.

TABLE I
CHEMICAL COMPOSITION (Wt%)[82,83]

	Rene' 95	NARloy Z
Al	3.550	---
P	0.010	---
Si	0.100	---
B	0.012	---
S	0.002	---
C	0.150	---
Co	8.000	---
Ti	2.500	---
Cb	3.560	---
W	3.570	---
Cr	13.800	---
Zr	0.040	0.500
Fe	0.130	---
Mo	3.500	---
Mn	0.100	---
Ni	Bal.	---
Ag	---	3.000
Cu	---	Bal.

TABLE II.

TENSILE PROPERTIES[82,83]

	Temp. (°C)	Ex 10^{-3} (MPa)	0.2% YLD (MPa)	UTS (MPa)	RA-%
Rene '95 (Cast + Forged)	20	---	1317.0	1613.0	11.8
	650	175.2	1207.0	1448.0	12.4
NARloy Z	20	127.0	198.3	316.2	51.0
	538	98.6	130.0	152.7	41.5

TABLE III

LCF TEST DATA OF RENE '95 AT 650°C[82]

Spec. No.	Test Type*	N_f (Cycl)	$\Delta\epsilon_t$ (%)	$\Delta\epsilon_p$	σ_{max} (KSI)	σ_{min}	$\Delta\sigma$	σ_{rel} Ten	σ_{rel} Comp	t_f (hrs)
21	PP	203	2.2	0.79	180	190	370			0.17
17	PP	234	2.0	0.53	178	195	373			0.20
18	PP	307	1.8	0.408	175	186	361			0.26
22	PP	461	1.6	0.31	168	173	341			0.38
240	PP	463	1.6	0.285	161	173	334			0.39
26	PP	784	1.4	0.217	156	164	320			0.65
27	PP	1629	1.2	0.104	140	146	286			1.36
268	PP	2369	1.2	0.006	140	148	288			2.14
30	PP	16215	0.9	0.012	107	125	232			13.50
234	PP	19160	0.9	0.013	99	134	233			15.97
235	PP	22364	0.9	0.0085	99	129	228			18.64
239	PP	28697	0.88	0.013	107	120	227			23.91
245	cp(1/0)	171	2.0	0.67	171	194	365			2.99
5	cp(1/0)	255	1.8	0.522	161	187	348	19.1		4.47
10	cp(1/0)	257	1.6	0.297	160	191	351	8.9		4.51
7	cp(1/0)	748	1.4	0.206	138	178	316	8.0		13.09
12	cp(1/0)	1289	1.2	0.089	129	166	295	1.67		23.02
39	cp(1/0)	1781	1.1	0.089	108	154	262	4.8		31.17
38	cp(1/0)	5013	1.0	0.49	101	148	249	1.5		87.72
233	cp(1/0)	6519	1.0	0.61	89	158	247	1.9		114.08
33	cp(1/0)	9609	1.0	0.38	82.8	159	241.8	0.51		168.15
237	cp(1/0)	16418	0.9	0.046	70.3	152	222.3	1.20		287.57
228	cp(10/0)	481	1.4	0.185	130	191	321	7.56		80.57
40	cp(10/0)	1705	1.2	0.126	108	178	286	6.20		285.58

TABLE III (CONTINUED)

LCF TEST DATA OF RENE '95 AT 650°C[82]

Spec. No.	Test* Type	N_f (Cycl)	$\Delta\varepsilon_\tau$ (%)	$\Delta\varepsilon_p$	σ_{max} (Ksi)	σ_{min}	$\Delta\sigma$	σ_{rel} Ten	σ_{rel} Comp	t_f (hrs)
6	pc(0/1)	207	1.8	0.429	178	181	359		15.0	3.5
11	pc(0/1)	209	1.6	0.468	162	161	323		15.8	3.66
14	pc(0/1)	219	1.6	0.324	177	174	351		10.7	3.83
8	pc(0/1)	413	1.4	0.292	165	158	323		6.2	7.3
13	pc(0/1)	846	1.2	0.098	156	140	296		2.3	14.8
241	pc(0/1)	1940	1.1	0.049	141	130	271		1.4	33.95
16	pc(0/1)	3093	1.0	0.0103	124	123	247		0.4	54.12
238	pc(0/1)	4619	0.9	0.029	127.4	101.4	228.8		1.4	80.83
222	pc(0/10)	224	1.4	0.136	176	155	331		5.0	37.5
41	pc(0/10)	283	1.2	0.185	164	117	281		14.0	47.4
253	pc(0/10)	1397	1.0	0.0305	141	110	251		0.7	234.0
1	cc(1/1)	156	1.8	0.55	181	196	377	28.6	21.6	5.19
2	cc(1/1)	238	1.6	0.35	170	184	354	18.6	14.0	8.07
32	cc(1/1)	358	1.4	0.20	150	172	322	9.7	7.1	12.13
9	cc(i/1)	959	1.2	0.12	135	154	289	7.5	8.81	32.48
4	cc(1/1)	1215	1.0	0.11	120	134	254	10.8	6.7	41.52
15	cc(1/1)	1288	1.0	0.078	117	136	253	6.2	5.1	43.65
229	cc(1/1)	5277	0.9	0.025	95	128	223	0.0	0.0	179.42
28	cc(10/10)	115	1.8	0.70	179	193	372	54.6	47.7	38.41
31	cc(10/10)	199	1.4	0.50	158	171	329	49.0	43.1	65.85
230	cc(10/10)	331	1.2	0.16	142	160	302	18.7	15.2	110.55

* (/): Tensile hold time/compressive hold time in minutes.

TABLE IV

APPLICABILITY AND LIMITATIONS OF THE LIFE MODELS FOR RENE '95[89]

Model	20 cpm	cp	pc	cc
Strain range Partitioning	Applicable	Underpredicts at long lives	Overpredicts 10 min. Holds	Applicable
Frequency Separation	Applicable	Underpredicts at short and long lives	Applicable	Applicable
Ostergren	Applicable	Underpredicts at long lives	Overpredicts 10 min. holds	Applicable
Damage Rate	Applicable	Underpredicts at long lives	Overpredicts at all lives	Applicable

TABLE V

LCF TEST DATA OF NARloy Z AT 538°C[83]

Spec. No.	Test* Type	N_f (Cycl)	$\Delta\varepsilon_t$ (%)	$\Delta\varepsilon_p$	ε_{ten} (%s^{-1})	ε comp	σ_{max} (MPa)	σ_{min}	$\Delta\sigma$	σ_{rel} Ten	σ_{rel} Comp	t_f (hrs)
118	PP(LR)	116	2.6	2.42	0.004	0.004			177			42
117	PP(LR)	787	0.9	0.72	0.004	0.004			173			101
23	PP(HR)	339	2.6	2.27	1.0	1.0			325			0.53
21	PP(HR)	3586	0.9	0.64	1.0	1.0			255			1.8
42	PC(0/5)	337	2.6	2.42	0.2	0.2	127	138	265		85	30.5
43	PC(0/5)	2981	0.9	0.76	0.2	0.2	105	105	210		72	256.
40	cp(5/0)	75	2.6	2.42	0.2	0.2	128	143	271	76		6.8
38	cp(5/0)	262	0.9	0.73	0.2	0.2	110	122	232	60		22.5

*
LR: low strain rate
HR: high strain rate
0/5: 5 min hold at compression
5/0: 5 min hold at tension

TABLE VI

CONTROLLING DAMAGE MODES AND POSSIBLE APPLICABLE FATIGUE

LIFE MODELS FOR SELECTED TEST TYPES FOR NARloy Z AT 538°C

	TEST TYPE			
	Continuous Cycling		Tensile Hold (or Slow-Fast)	Compressive Hold (or Fast-Slow)
	High $\dot{\epsilon}$	Low $\dot{\epsilon}$		
fracture surface	transgranular	intergranular	intergranular	transgranular
interior	minor grain boundary damage	minor grain boundary damage	extensive grain boundary cracking	minor grain boundary damage
environment	local to the surface	deep into the matrix	going into the matrix	local to the surface
controlling damage mode	cyclic strain damage	environmental damage	creep and environmental damage	cyclic strain damage
model	Coffin-Manson law	Coffin's frequency modified model	may be SRP model	Coffin-Manson law
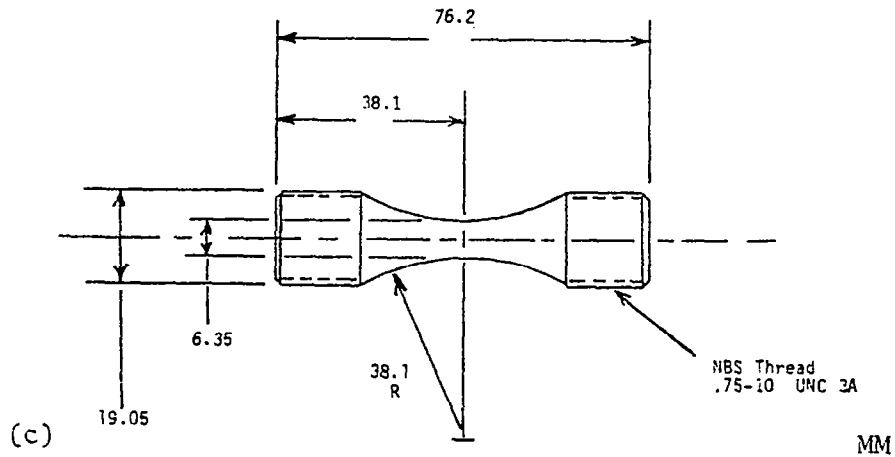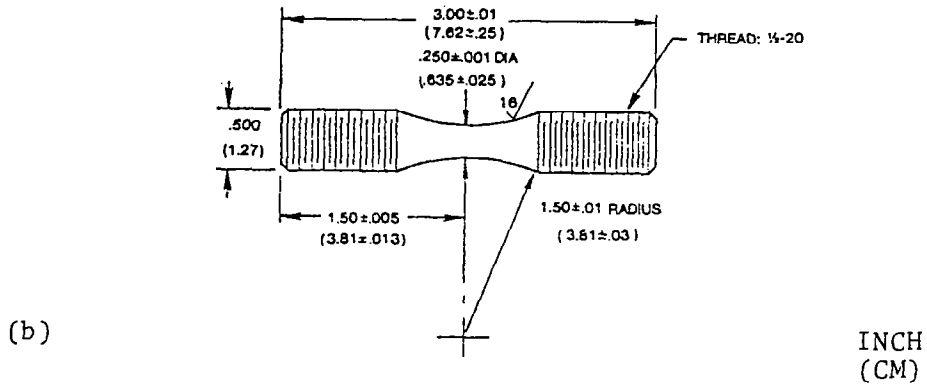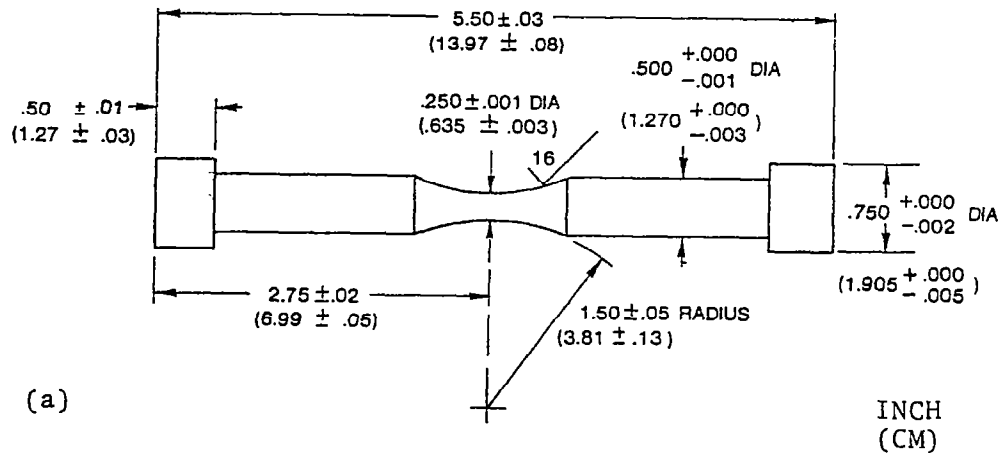
Fig. 1. Hourglass fatigue specimens of Rene' 95 with botton-head (a) and threaded ends (b). Specimen of NARloy Z with threaded ends (c). Unit used for each specimen is indicated on its lower right corner.

(a) PP cycle; high-
   strain rate.

(b) CP cycle;
   stress-hold.

(c) CP cycle;
   strain-hold.

(d) CP cycle;
   low/high
   strainrate.

(e) PC cycle;
   stress-hold.

(f) PC cycle;
   strain-hold.

(g) PC cycle;
   high/low
   strainrate.

(h) CC cycle;
   stress-hold.

(i) CC cycle;
   strain-hold.

(j) CC cycle;
   low strainrate.
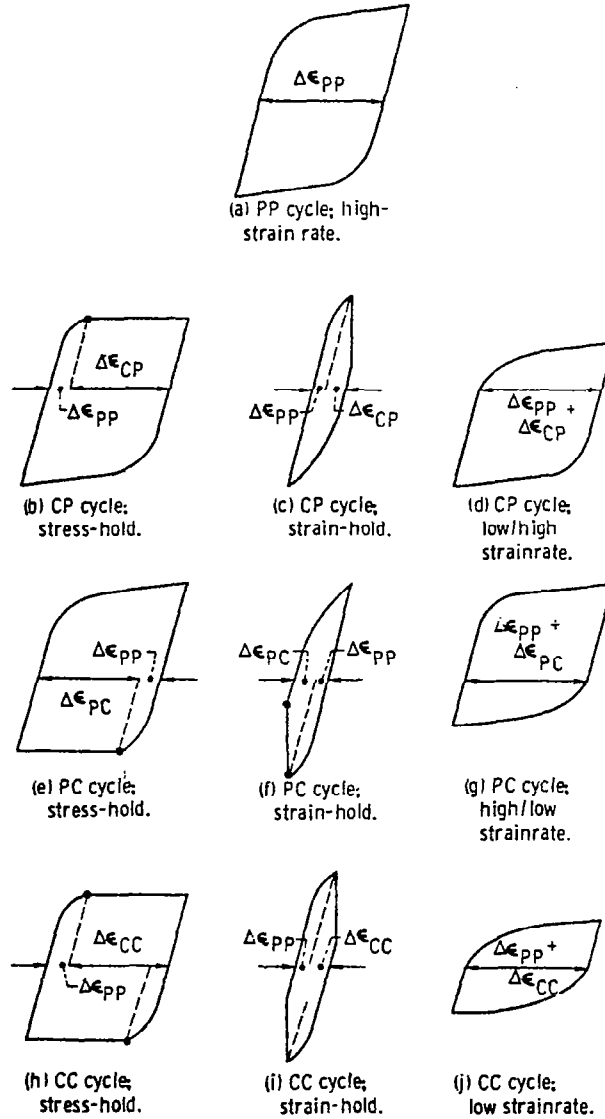
Fig. 2. Examples of isothermal test cycles
for testing strain-range partitioning model.[1]

-75-

CONTINUOUS STRAIN CYCLING
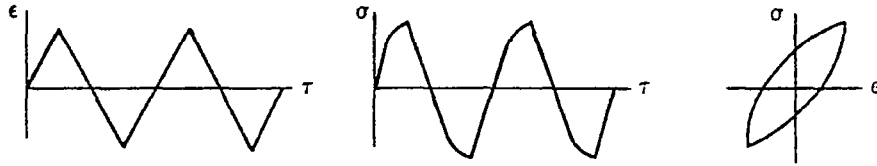
TENSION STRAIN HOLD
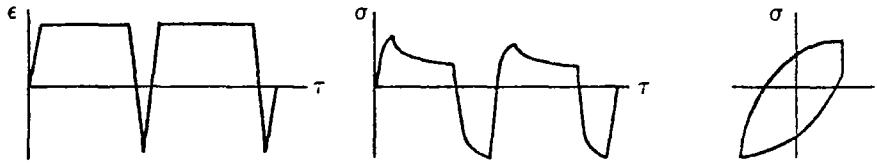
COMPRESSION STRAIN HOLD
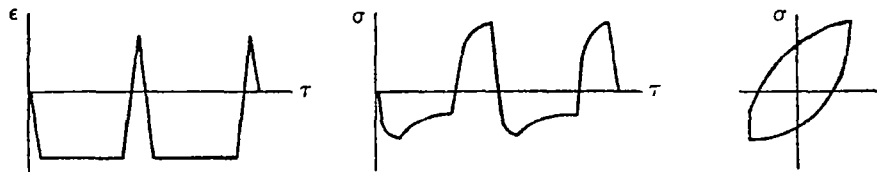
TENSION AND COMPRESSION STRAIN HOLD
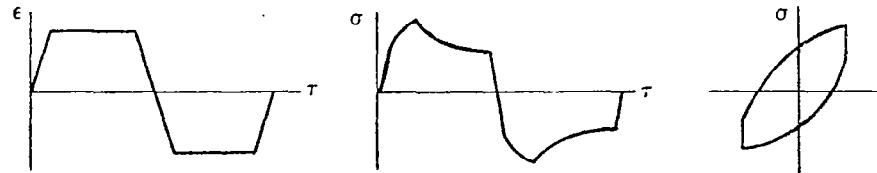
Fig. 3. Waveforms and resulting hysteresis loops
for tests under continuous cycling and with
strain hold times.
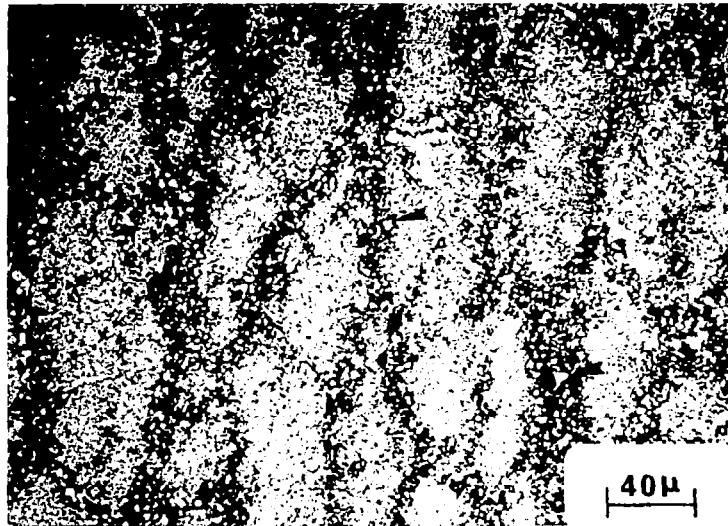
Fig. 4. Optical micrograph of necklace Rene' 95 showing
the warm worked grains and the necklace regions. Arrows
indicate MC carbides.
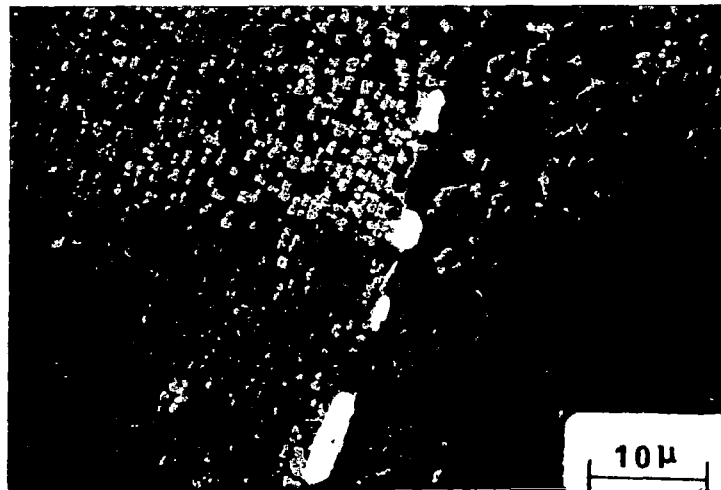
Fig. 5. SEM micrograph of the necklace structure showing
large γ' on the necklace grain boundaries and the inter-
mediate sized γ' in the warm worked grains. White
particles in the center are MC carbides.

Fig. 6. TEM micrograph of the necklace region showing the large γ' (a) on the grain boundaries and the fine γ' inside the grains.
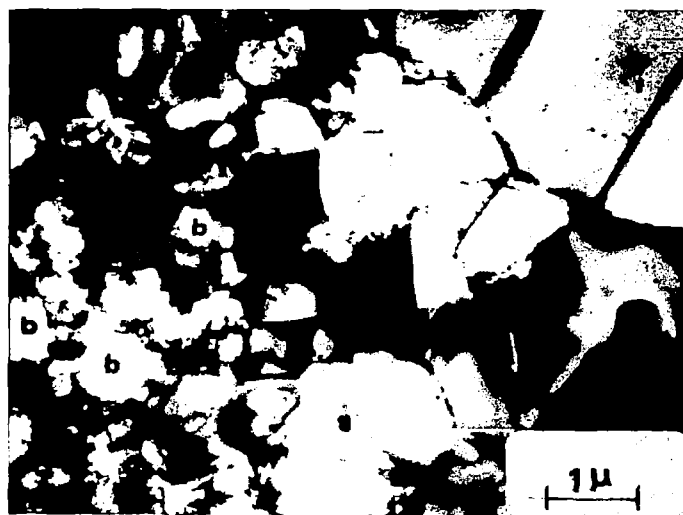
Fig. 7. TEM micrograph of both a warm worked grain (left) and the necklace region surrounding it (right). Note the dislocation substructure around the intermediate γ' (b) in the warm worked grain.
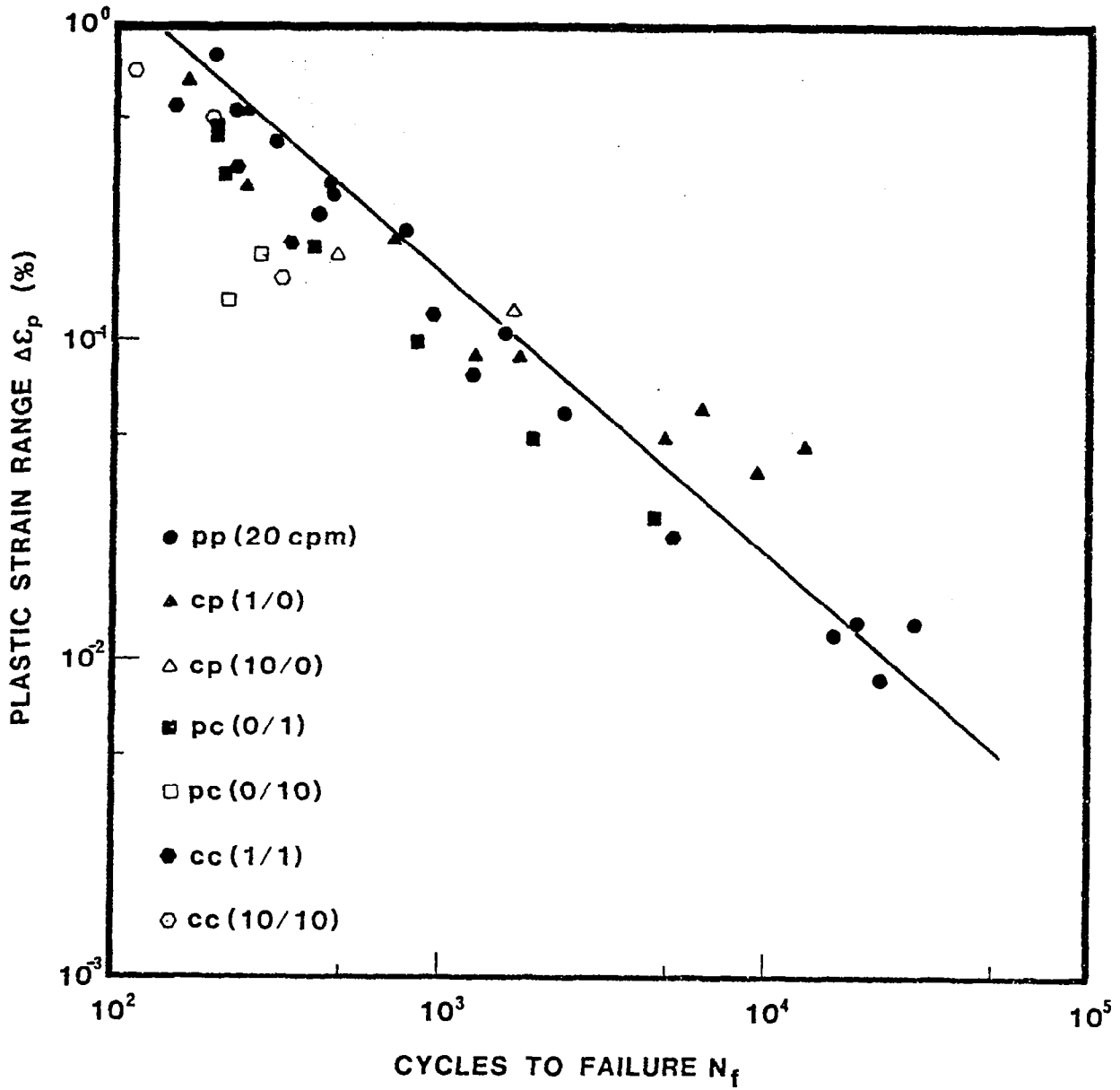
Fig. 8. Coffin-Manson plot for Rene' 95 at 650°C under continuous cycling and with strain holds. The straight line represents the relationship for continuous cycling tests at 20 cpm. (82)
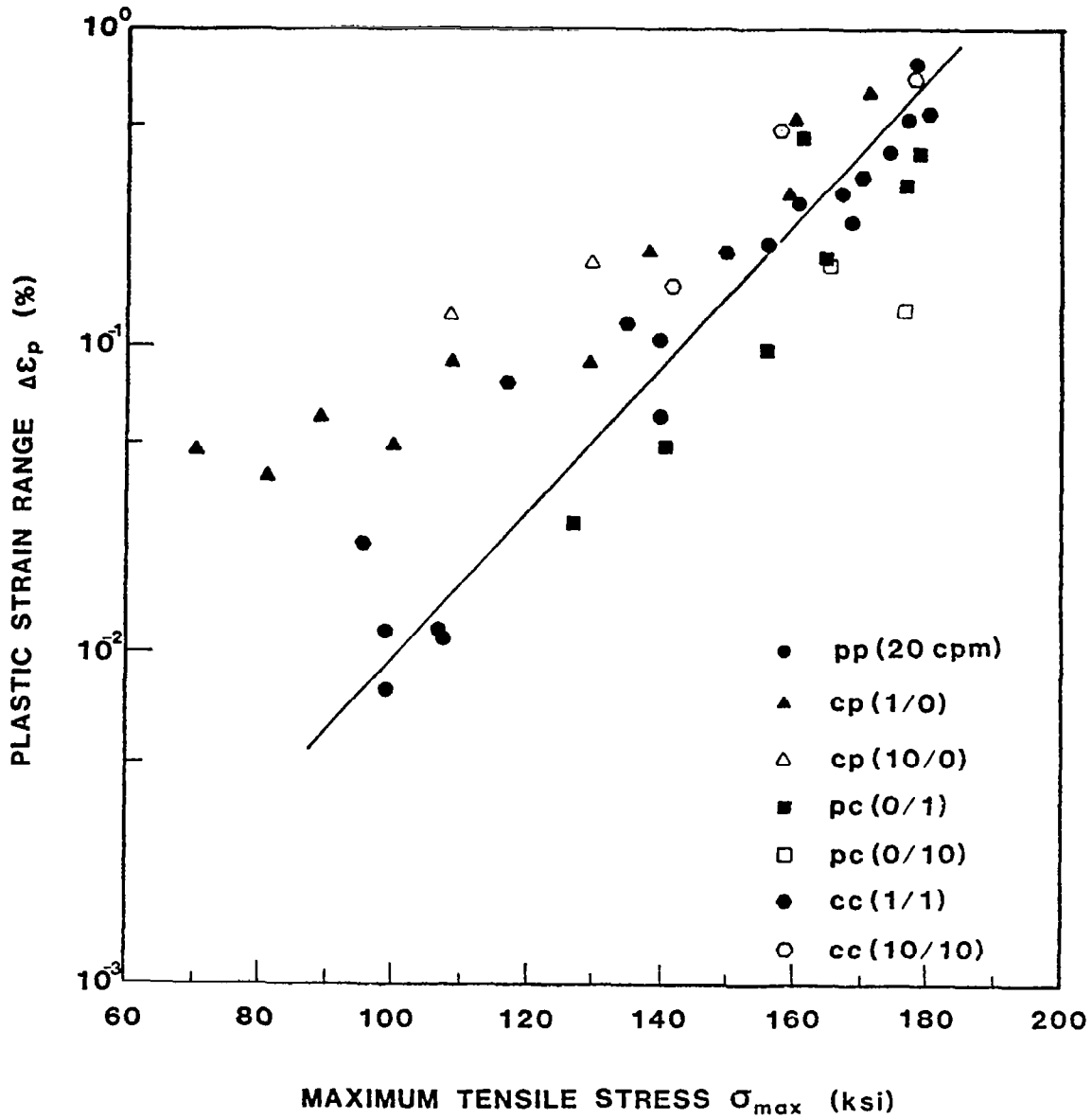
Fig. 9. The dependence of maximum tensile stress on plastic strain range for different cycle types. Note the shift in maximum tensile stress developed during hold time compared to continuous cycling (represented by the straight line). [82]
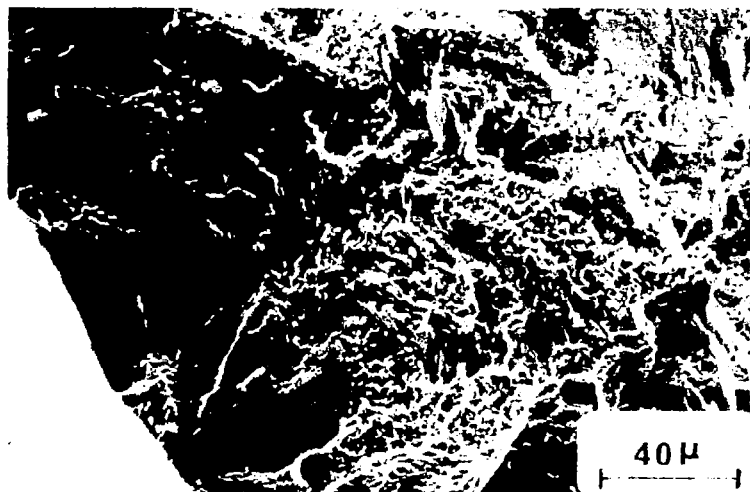
(a)
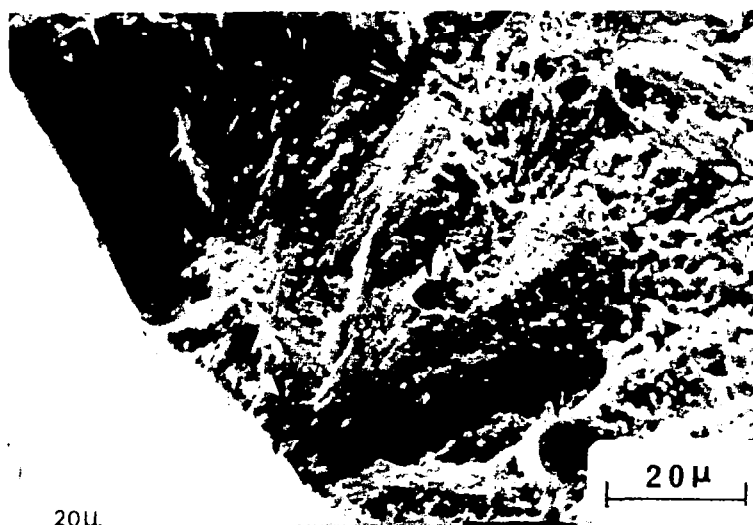
(b)

Fig. 10. Typical crack initiation region fór specimens
tested at high strain ranges under continuous cycling.
In (a) there is a transgranular initiation followed by
a mixed mode of propagation. In (b) crack origin is
shown at higher magnification with faint striations and
MC carbides (arrows) visible on the fracture surface.
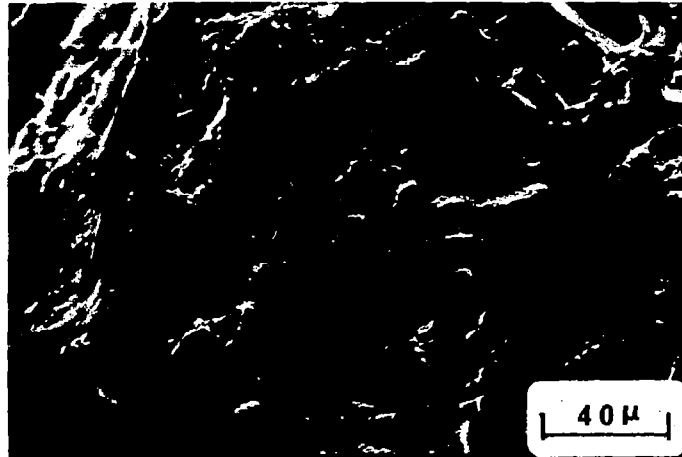
Fig. 11. Crack initiation region where the crack probably
had initiated intergranularly and further propagated mainly
by transgranular mode. Note that the striation like
feature are quite brittle in nature.

Fig. 12. SEM micrograph of a longitudinal section showing
a crack which had initiated transgranularly. Note the
crack changed direction upon travelling across a single
warm worked grain or crossing the necklace regions.
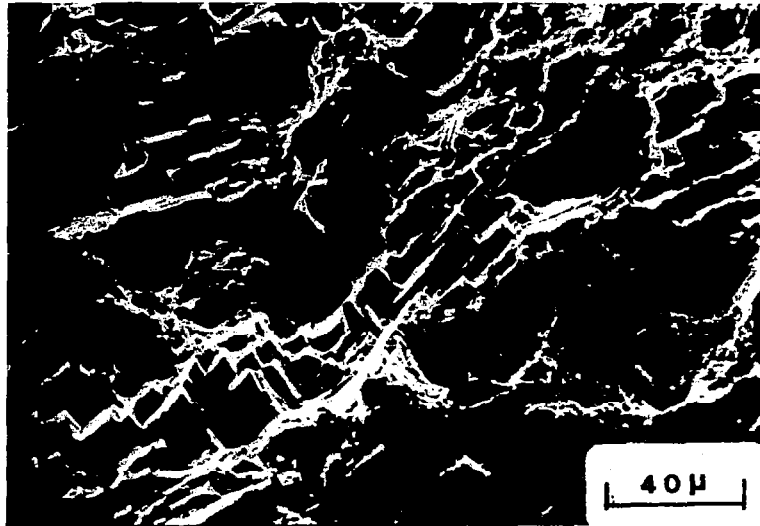
Fig. 13. Typical facets present on the fracture surface
in the later stage of crack propagation.
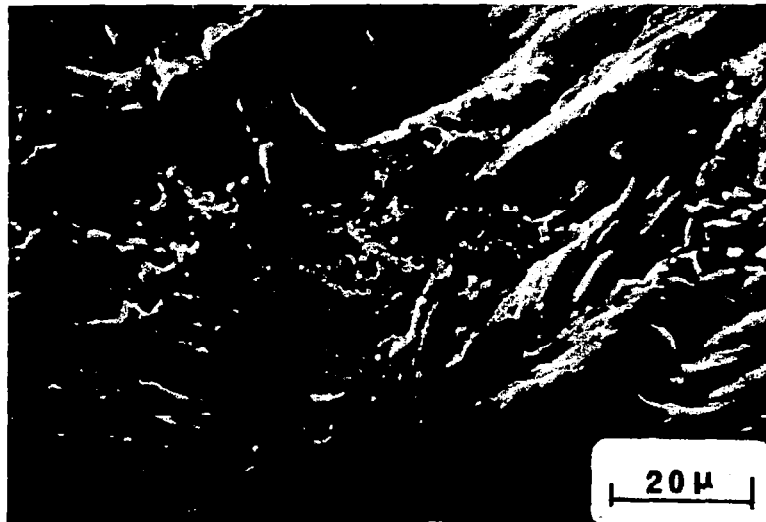
Fig. 14. Typical crack initiation at a surface MC carbide
(arrow) which had fallen off during testing.

Fig. 15. Fracture surface of continuously cycled specimens with Δε=0.9%. Note the dual mode of cracking, transgranular in the large warm worked grains and intergranular through the necklace regions. Slip traces are revealed in the grain where crack initiated. Arrow indicates the initiation site.
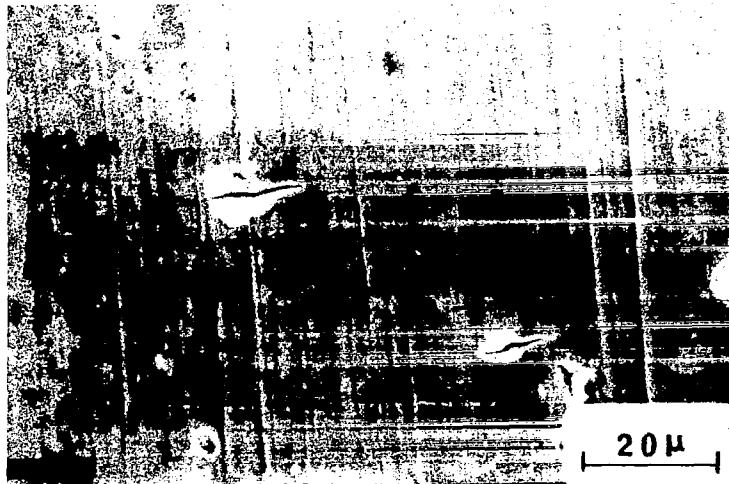
(a)
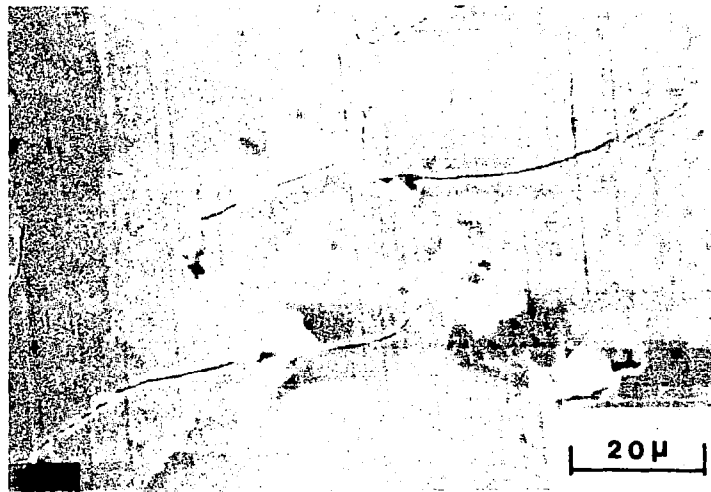
(b)

Fig. 16. SEM micrograph showing cracking of MC carbides
on the gage surface of specimens. In (a) two surface MC
carbides had ruptured during testing while (b) shows
further propagation into the matrix. The longitudinal
marks are due to the finish machining operation.
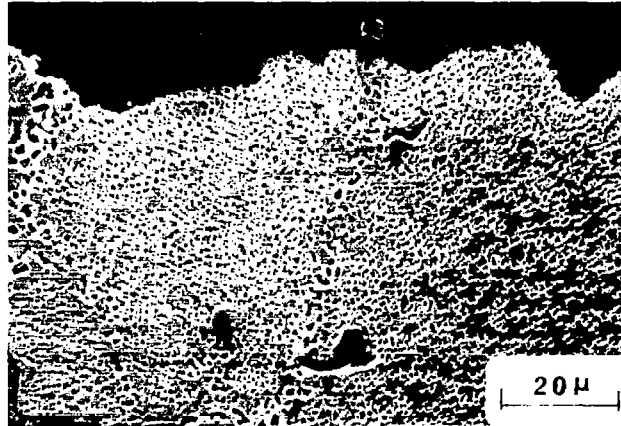
Fig. 17. SEM micrograph of longitudinal section showing fractured MC carbides in the interior of the specimen.
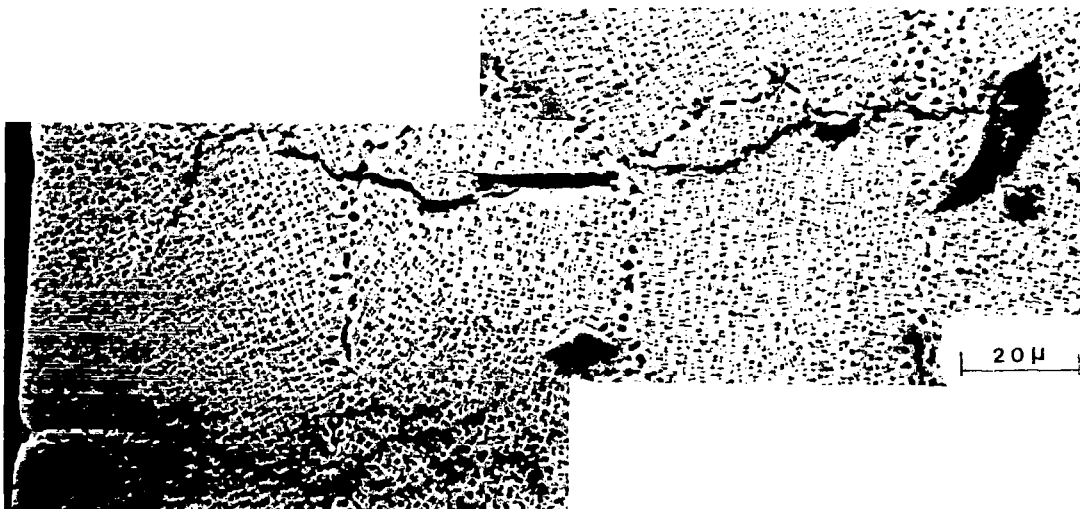
Fig. 18. Internal crack occasionally observed in specimens tested at high strain ranges, probably initiated due to cracking of internal MC carbides. The crack on the left is surface associated.
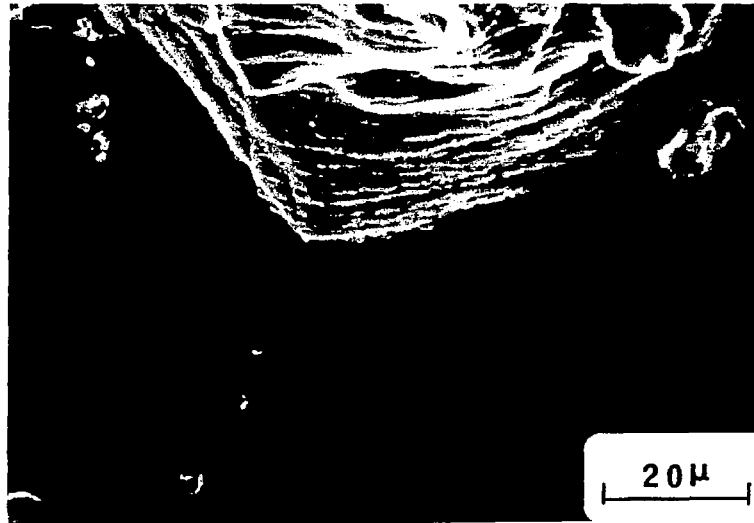
Fig. 19. SEM micrograph of gage surface showing slip
offsets in the crack propagation region.

Fig. 20. The edge of the fracture surface away from the
crack origin parallel to the slip offsets on the gage
surface.
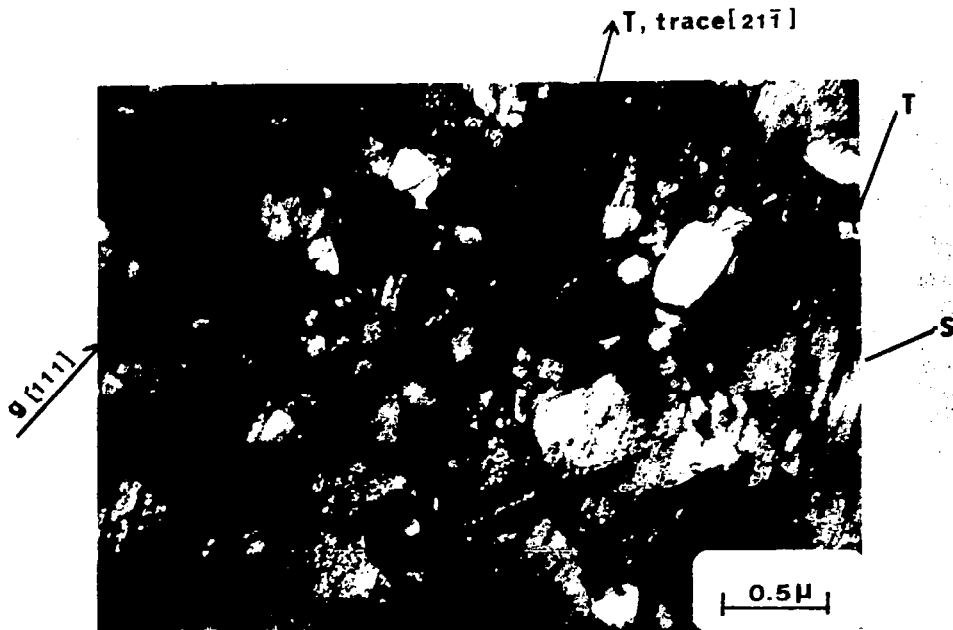
Fig. 21. Deformed microstructure of Rene' 95 in a single warm worked grain showing microtwins (trace T) and slip bands (trace S).
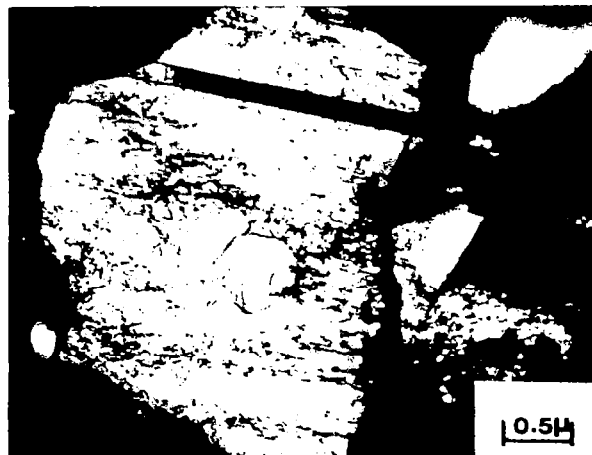
Fig. 22. Planar slip in a necklace grain of Rene' 95.

(a)

(b)

40μ
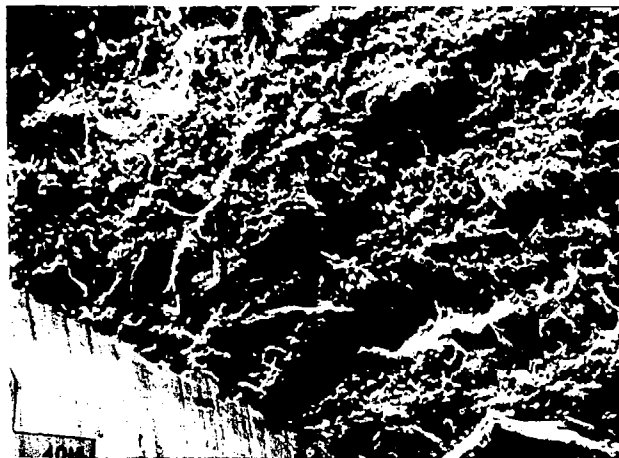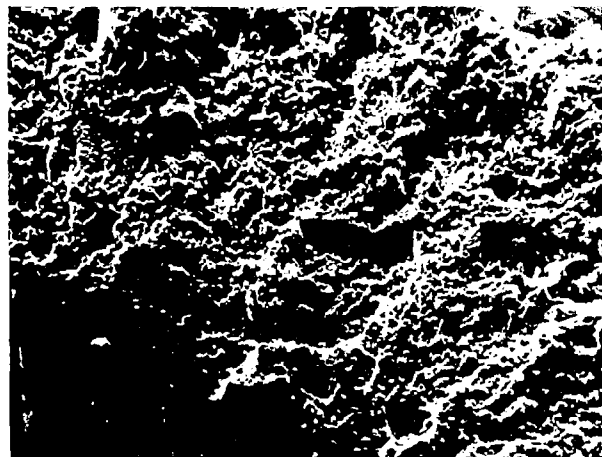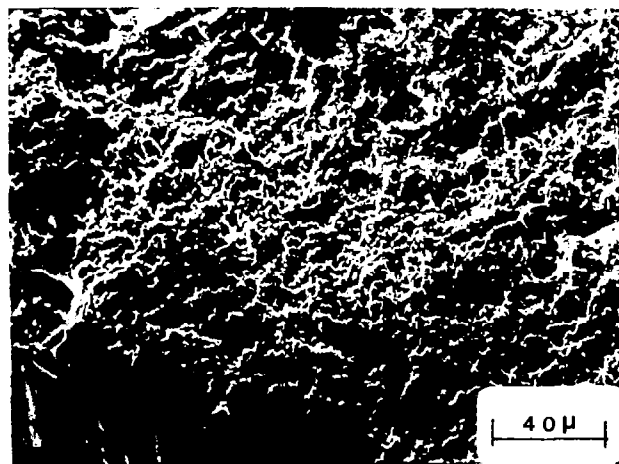
(c)

Fig. 23. Intergranular crack initiation
and early propagation in specimens tested
at $\Delta\varepsilon_t$=1.4% under tensile hold (a),
compressive hold (b) and balanced hold(c).

-89-
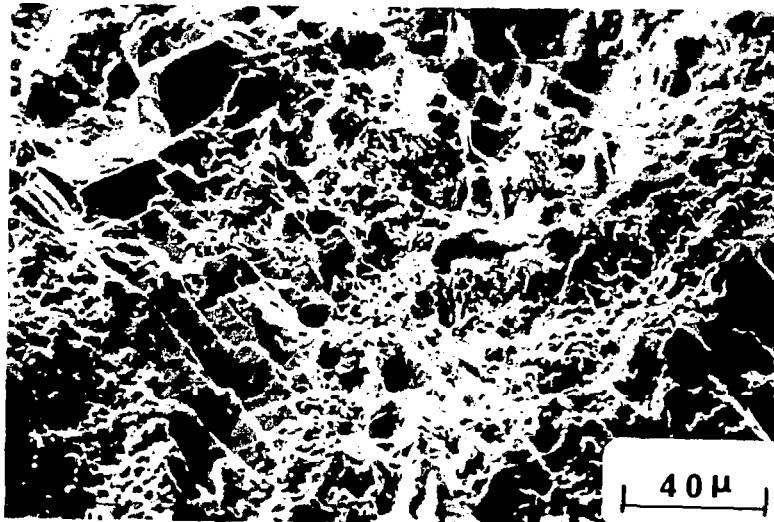
(a)
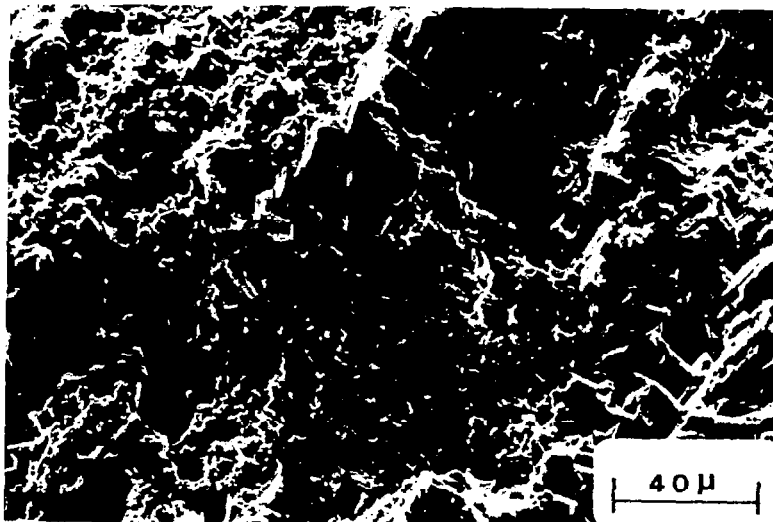
(b)

Fig. 24. Mixed mode of cracking in specimens tested under
hold times showing fracture features, facets (a) and
striation like feature (b) in the warm worked grains.
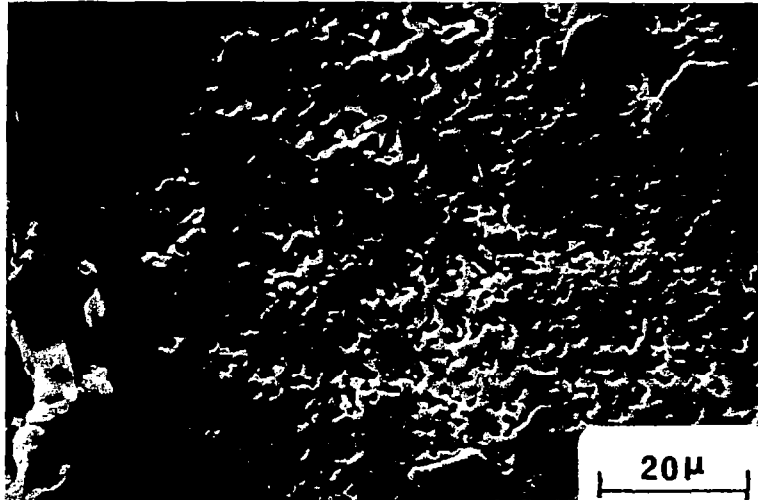
Fig. 25. Crack initiation in the necklace region for hold time tests.
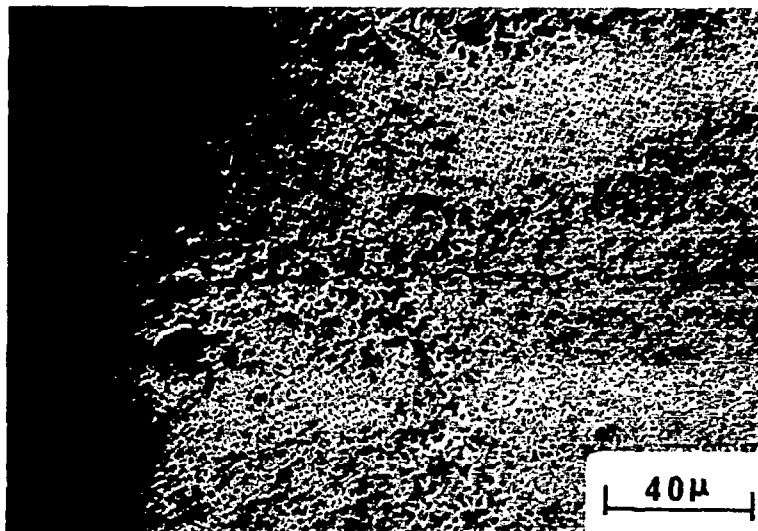
Fig. 26. A crack initiated transgranularly and propagated intergranularly before meeting a warm worked grain.
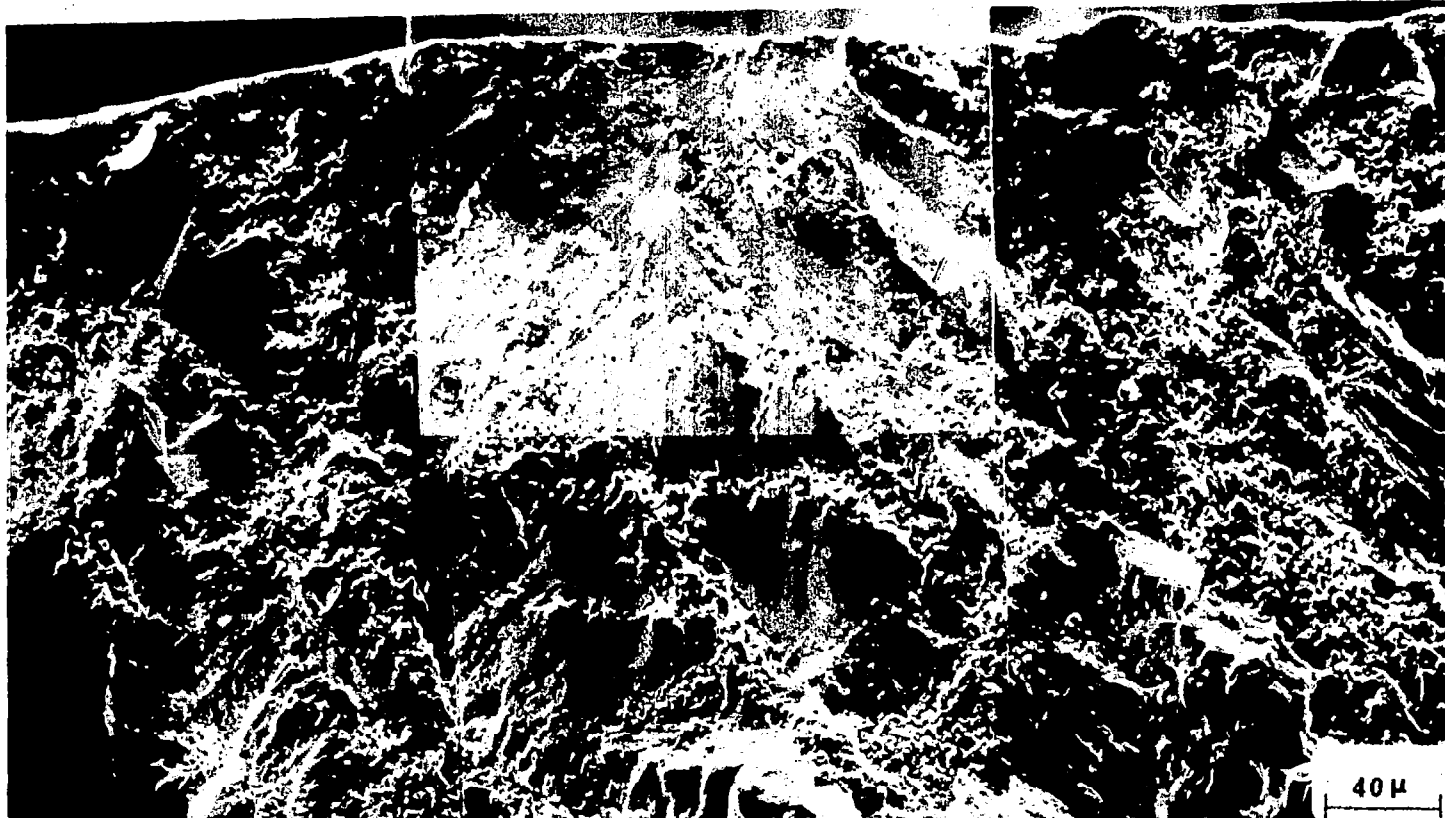
Fig. 27. Dual mode of cracking in specimen tested under tensile hold with $\Delta\varepsilon_t$=0.9%. This is typical for hold time tests at low strain ranges. Arrow indicates initiation site.
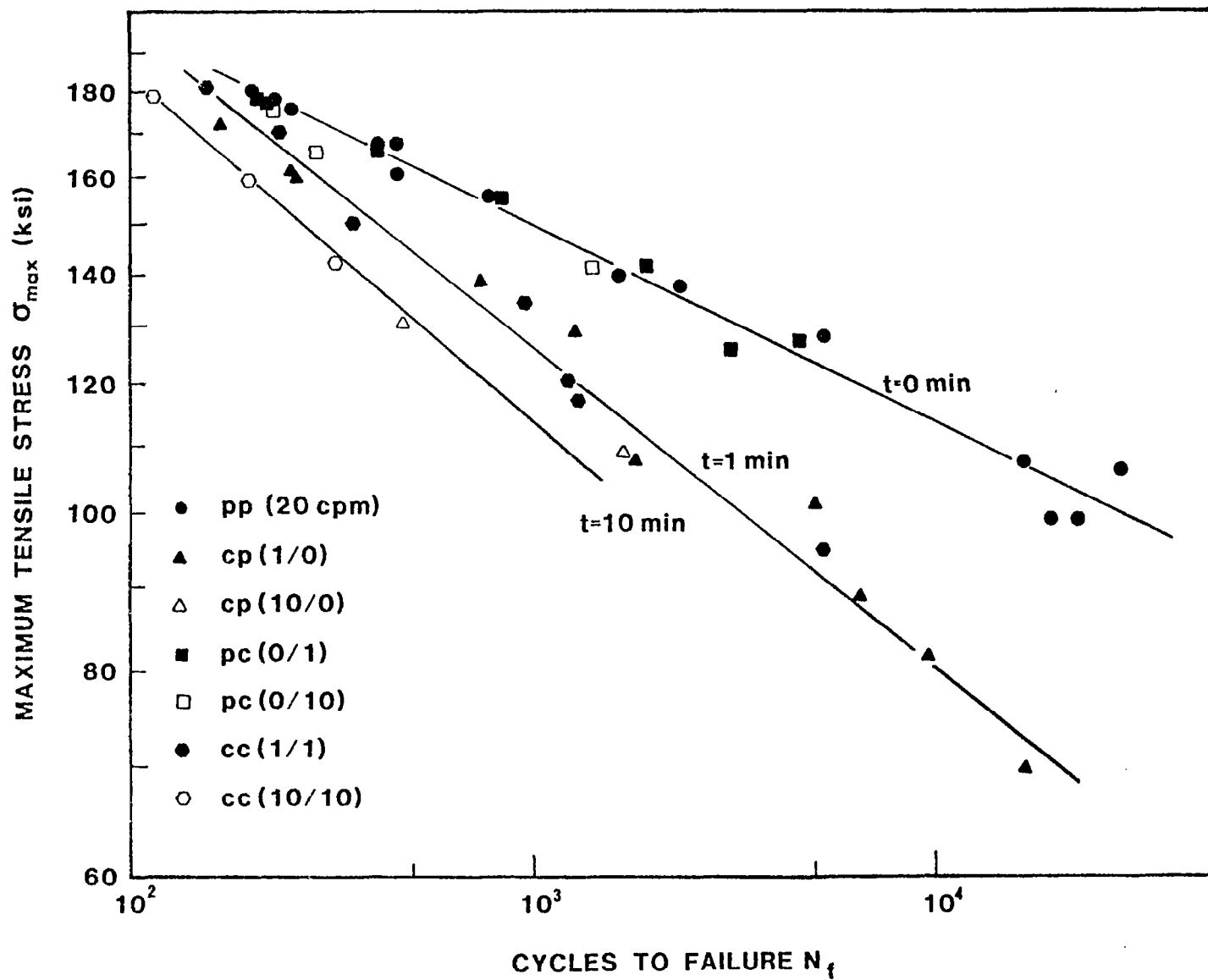
Fig. 28. Dependence of life on maximum tensile stress for all cycle types. All the data seem to fall into three lines corresponding to three tensile hold times. (82)
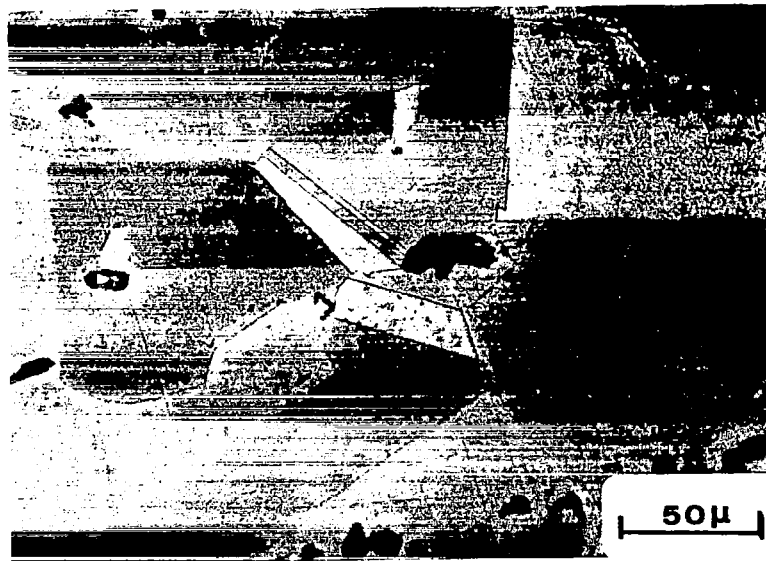
Fig. 29. Microstructure of NARloy Z showing intermetallic compound Cu-10 Ag-22.5 Zr and annealing twins.

(a)
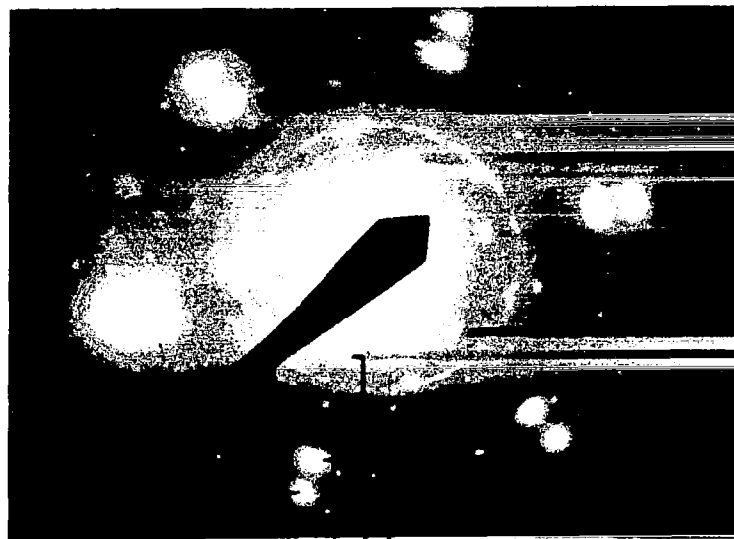
Cu   Cu$_2$O   Ag [rings]

(b)

Fig. 30. (a) TEM micrograph showing initial structure of
NARloy Z with larger precipitates Ag and relatively small
precipitates Cu$_2$O. (b) Diffraction pattern under (111).
The former give rise to rings while the latter,
superlattice spots.
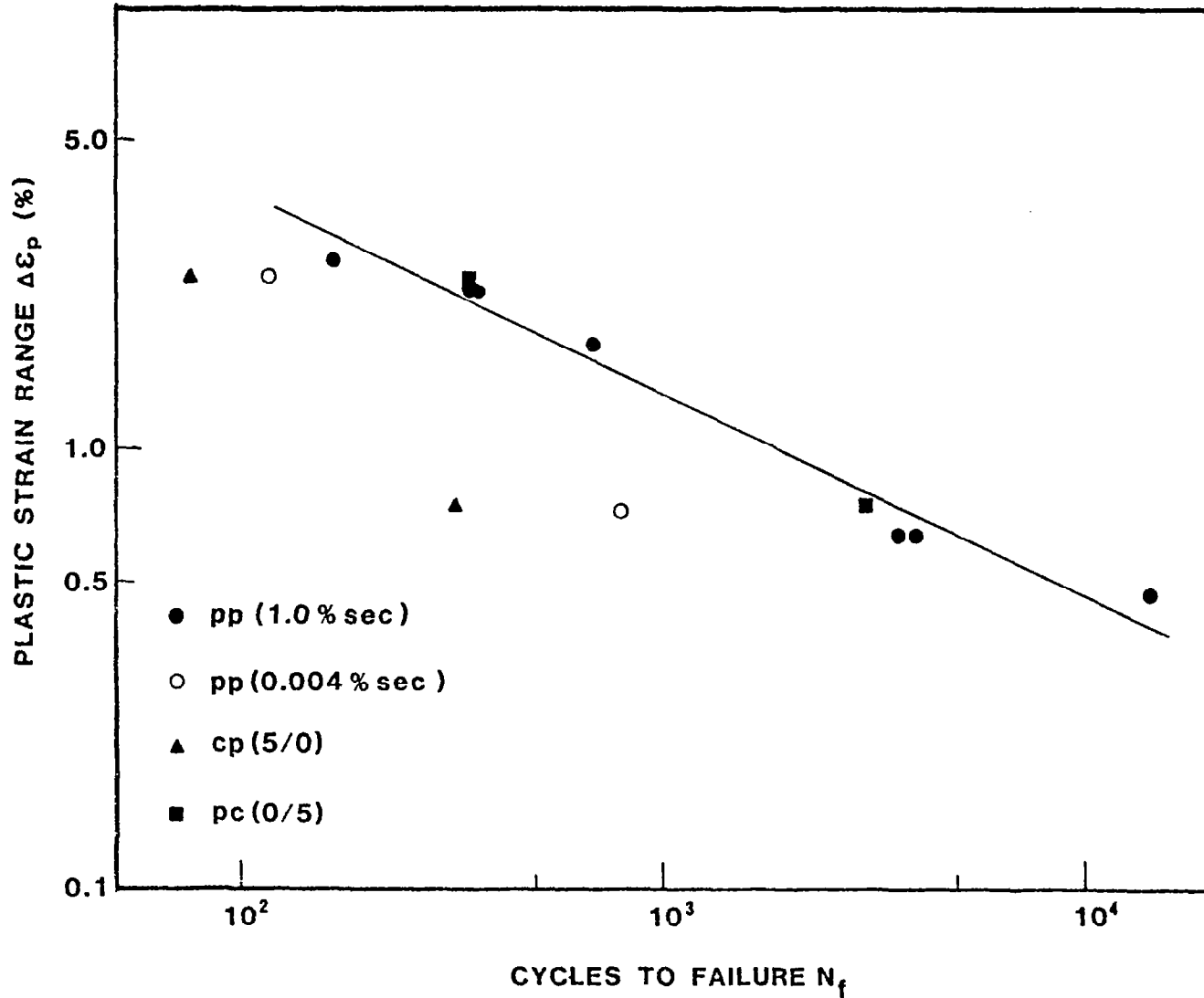
Fig. 31. Coffin-Manson plot for NARloy Z at 538°C under continuous cycling and with strain holds. The straight line represents the relationship for continuous cycling tests at 1.0 percent sec^{-1}. [83]
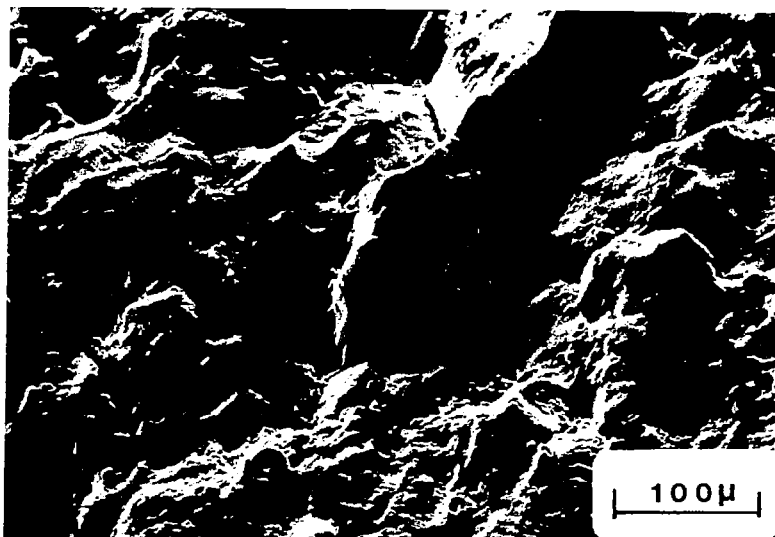
(a)
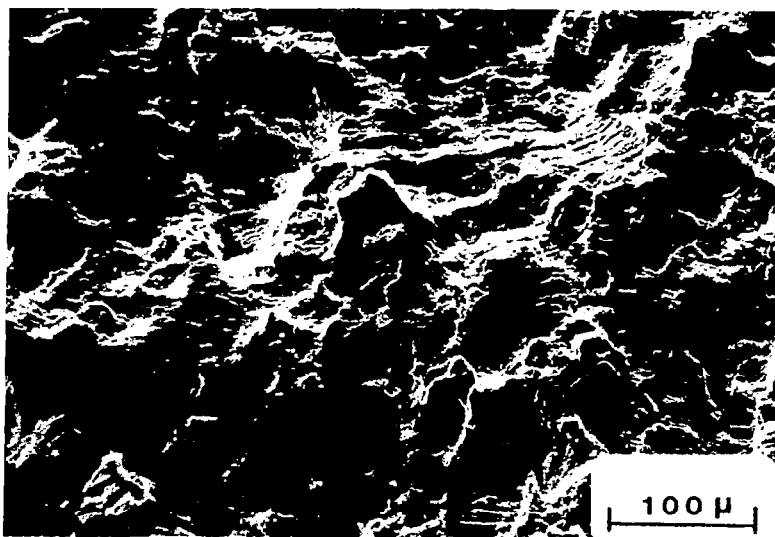
(b)

Fig. 32. Typical fracture feature for specimens tested at 1.0 percent sec^{-1}. (a) shows transition of cracking from intergranular to transgranular mode. (b) shows striations in the region of transgranular crack propagation.
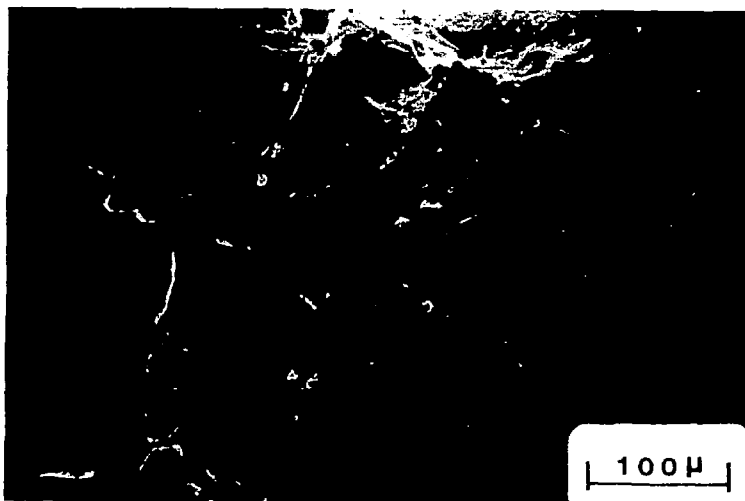
Fig. 33. Gage surface of specimens tested at 1.0 percent sec^{-1} showing grain boundary decohesion.

(a)

Fig. 34. (a) Longitudinal section of specimens tested at 1.0 percent sec^{-1} showing surface cracks ceased growing right after initiation.
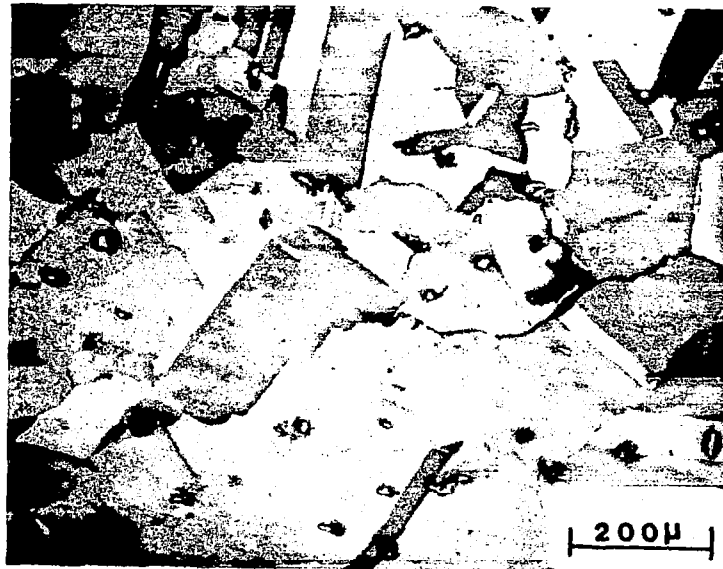
(b)
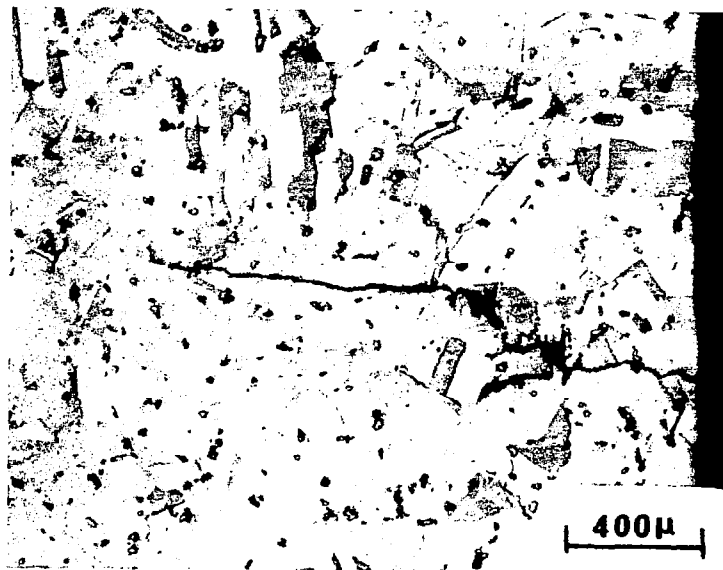
(c)

Fig. 34. (Continued) (b) shows a crack which had grown
two or three grains in depth. (c) shows a crack grew
like the main crack, transgranularly into the matrix.

[a]
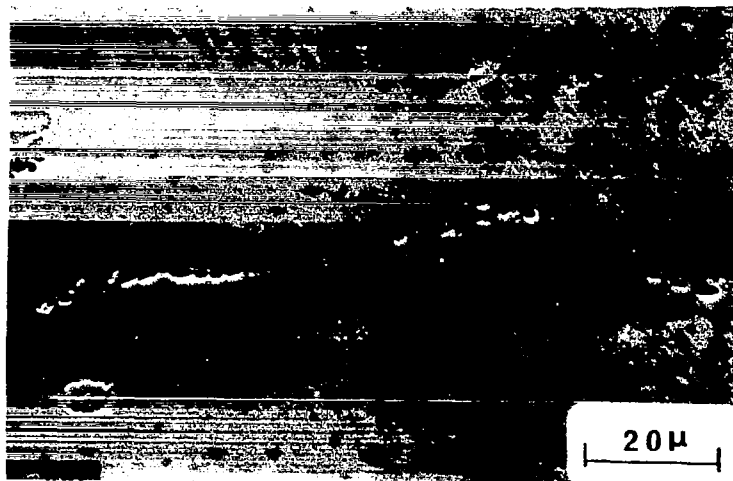
[b]

Fig. 35. Internal damage in specimen tested at $\dot{\epsilon}$=1.0% sec^{-1} and $\Delta\epsilon_t$=2.6% in the form of wedge cracks (a) and cavities (b).
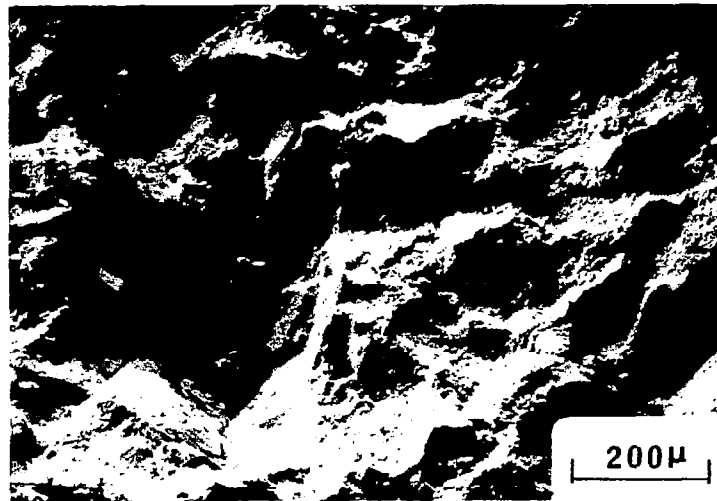
Fig. 36. Typical intergranular cracking for specimens tested at 0.004 percent sec^{-1}.
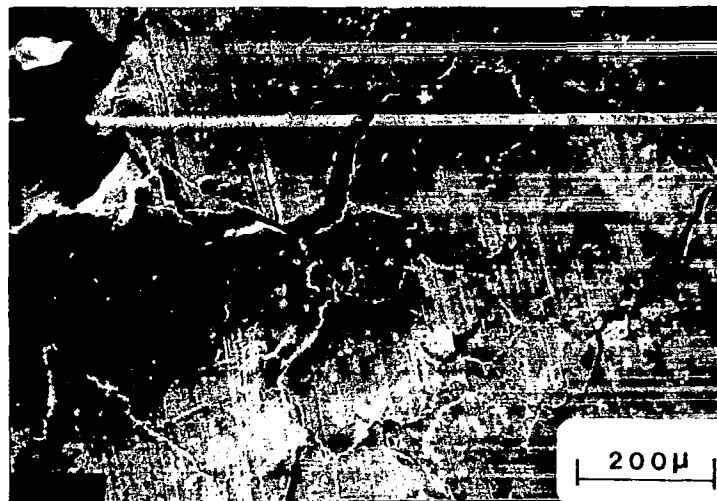
Fig. 37. Grain boundary cracking on the gage surface of specimens tested at 0.004 percent sec^{-1}.
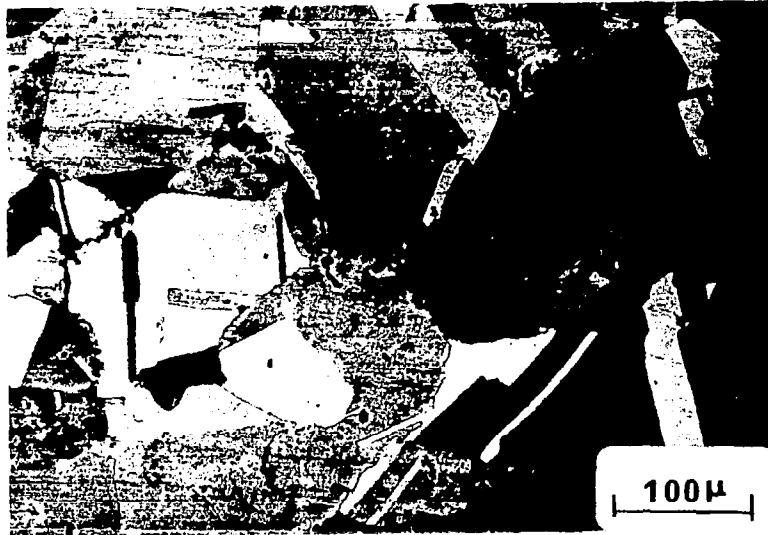
Fig. 38. Typical surface intergranular crack for specimens tested at 0.004 percent sec^{-1}.

Fig. 39. Typical internal damage for specimens tested at 0.004 percent sec^{-1}.
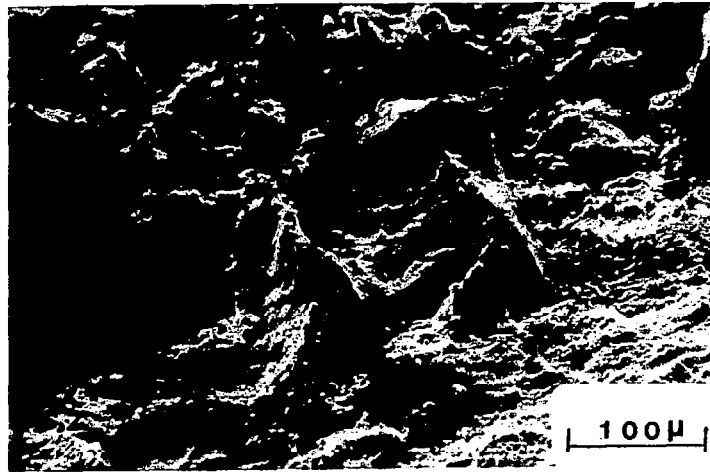
Fig. 40. Transition of cracking from intergranular to trans-
granular mode in specimens tested under compressive hold.
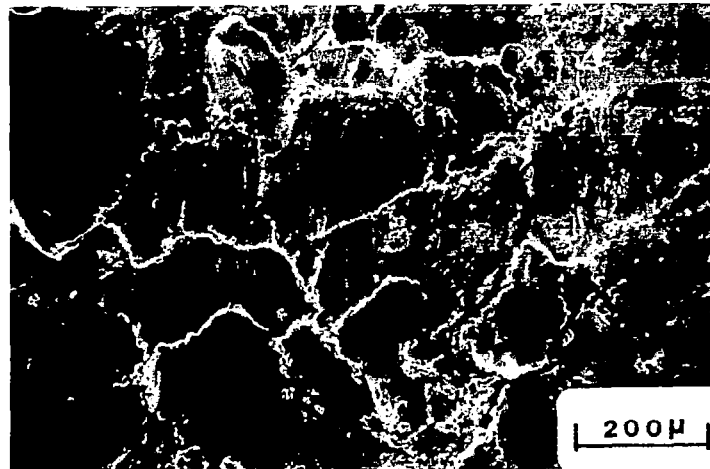
Fig. 41. Severe preferential grain boundary oxidation in
specimens tested under compressive hold.
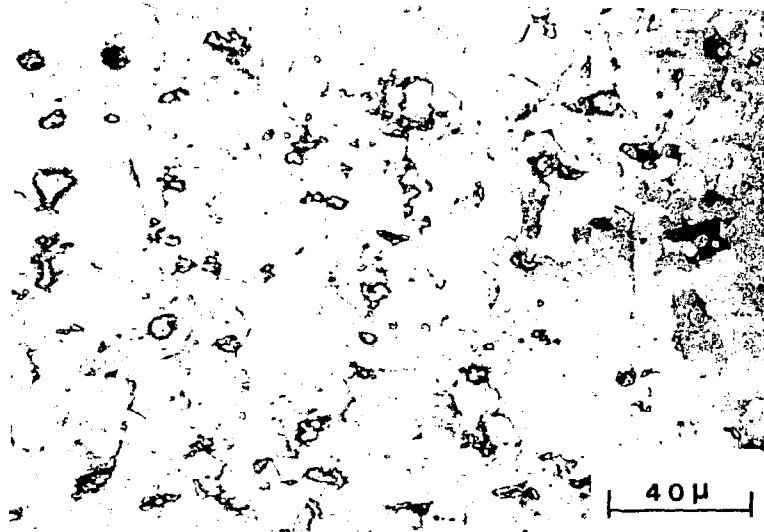
Fig. 42. Occurrence of recrystallization in the gage section of specimen tested under compressive at $\Delta\varepsilon_t$= 0.9%.
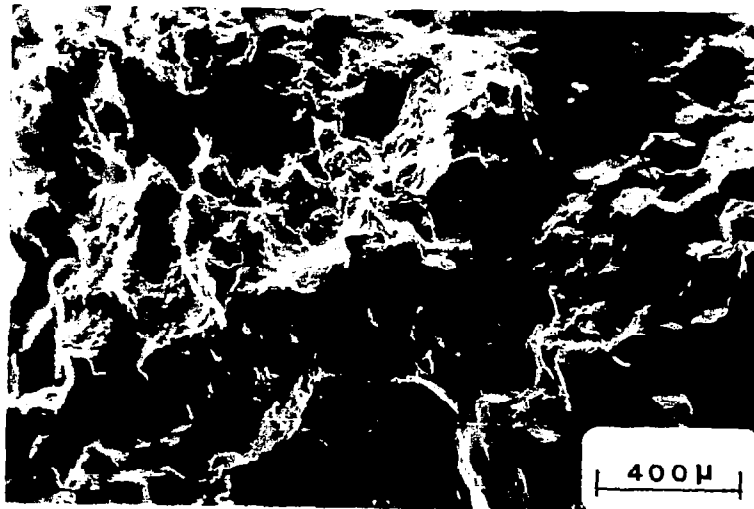
Fig. 43. Intergranular fracture on specimens tested under tensile hold.
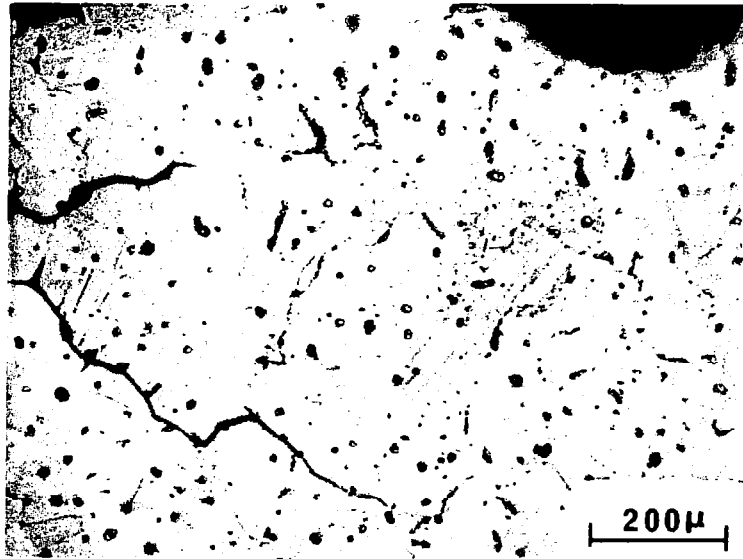
Fig. 44. Internal cracks in specimen tested under tensile
hold at $\Delta\varepsilon_t$= 2.6%.
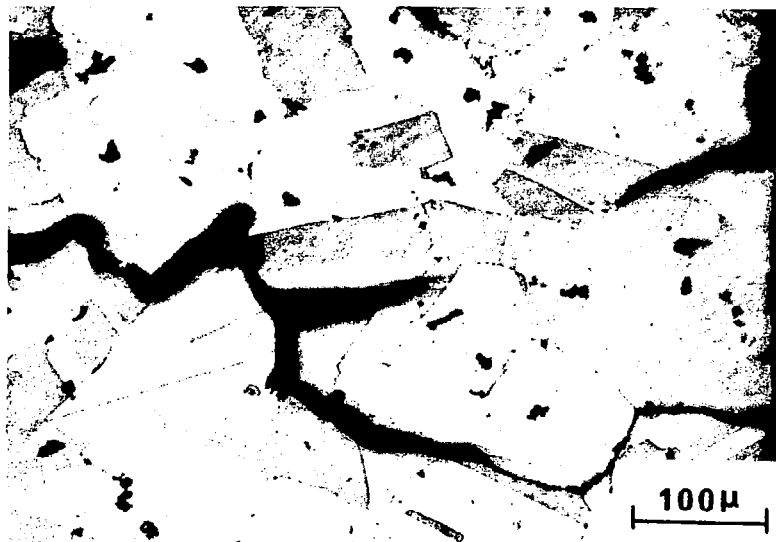
Fig. 45. Linkage of surface and internal cracks in specimen
tested under tensile hold at $\Delta\varepsilon_t$=0.9%.
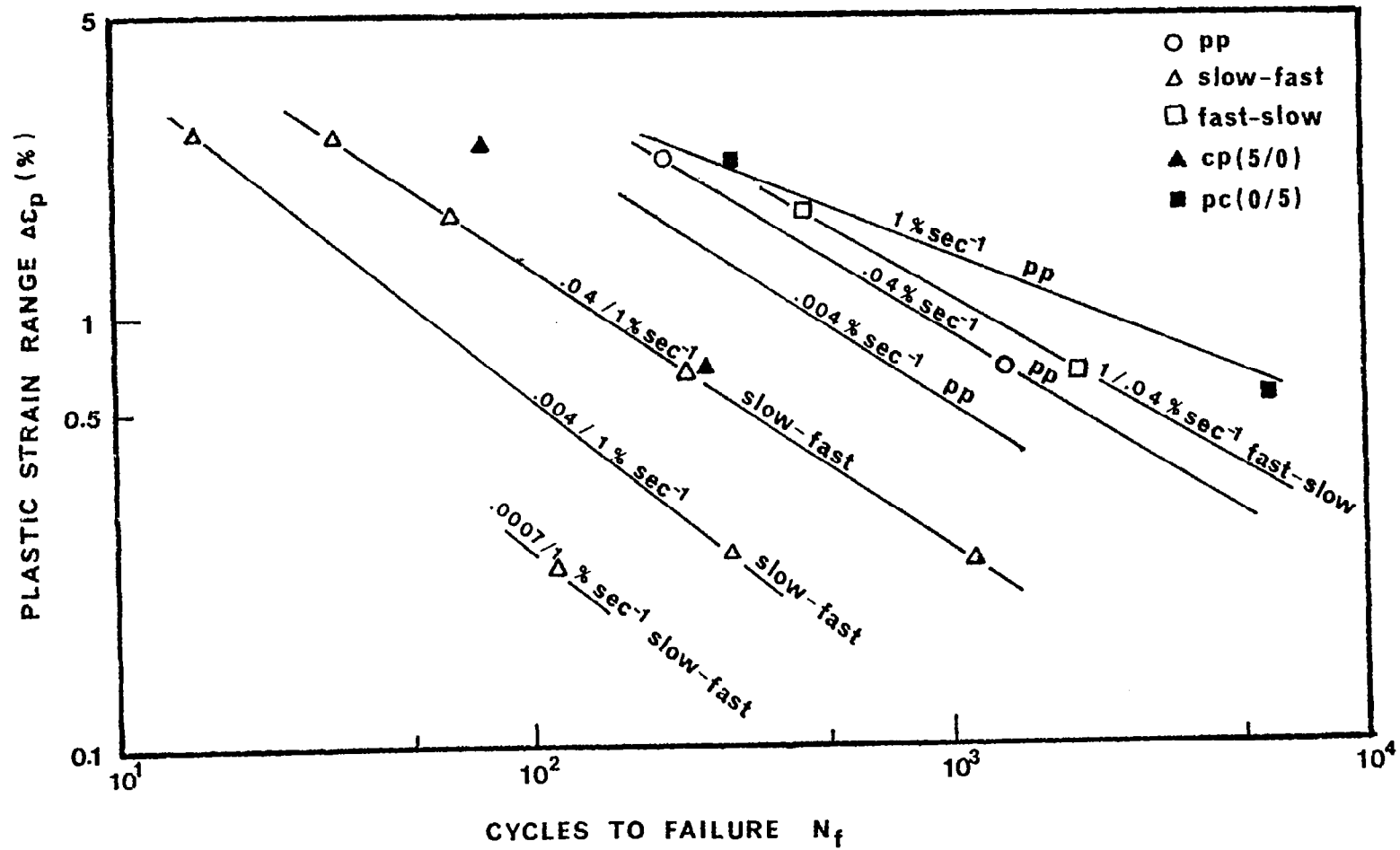
Fig. 46. Coffin-Manson plot for NARloy Z under continuous cycling at medium strain rate, slow-fast and fast-slow cycling (represented by open symbols). Data from Fig. 31 are superimposed also.[83]
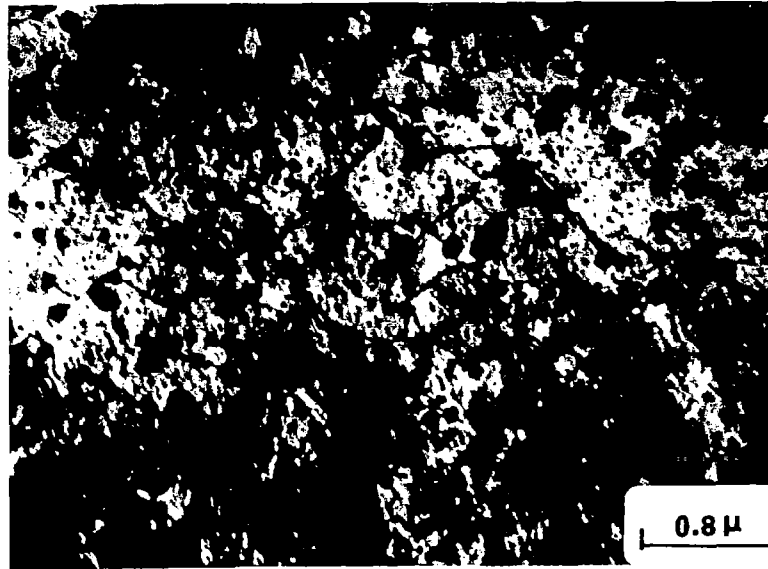
[a]
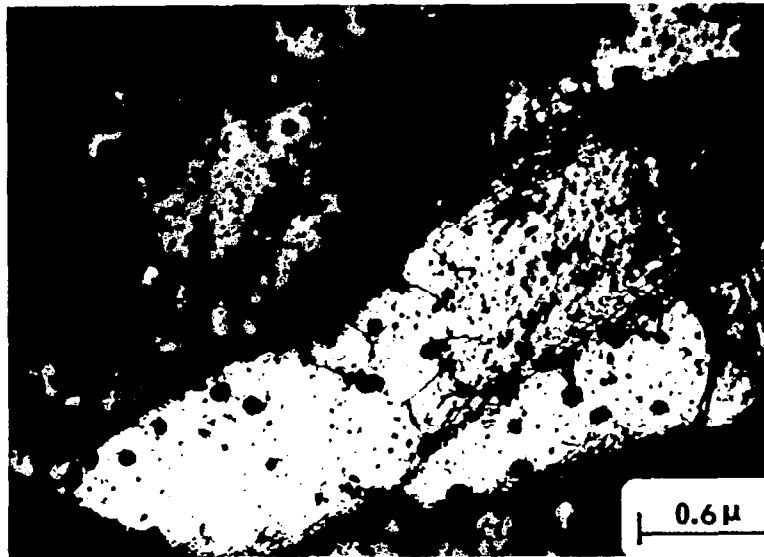
[b]

Fig. 47. TEM micrograph showing deformed microstructure of
NARloy Z tested under continuous at 0.004 percent sec^{-1}.
(a) shows a grain with random distribution of dislocations
and most of them were pinned by Ag precipitates. In (b),
in the same specimen subgrains had formed.

1. Report No. NASA CR-3543	2. Government Accession No.	3. Recipient's Catalog No.
4. Title and Subtitle HIGH TEMPERATURE LOW CYCLE FATIGUE MECHANISMS FOR A NICKEL-BASE AND A COPPER-BASE ALLOY		5. Report Date June 1982
		6. Performing Organization Code
7. Author(s) Chin-I Shih		8. Performing Organization Report No. None
		10. Work Unit No.
9. Performing Organization Name and Address University of Cincinnati Department of Materials Science and Metallurgical Engineering Cincinnati, Ohio		11. Contract or Grant No. NSG-3263
		13. Type of Report and Period Covered Contractor Report
12. Sponsoring Agency Name and Address National Aeronautics and Space Administration Washington, D.C. 20546		14. Sponsoring Agency Code 505-33-22

16. Abstract

Damage mechanisms were studied in nickel-base superalloy Rene' 95 and copper-base alloy NARloy Z, using optical, scanning and transmission in microscopy. Continuous cycling and strain hold time tests were performed at 650°C for Rene' 95 and at 538°C for NARloy Z under AGARD SRP program. Results showed that the two materials, having quite different microstructures and tensile properties, exhibited contrasting LCF behavior. In necklace Rene' 95, crack initiation was mainly associated with cracking of surface MC carbides, except for hold time tests at higher strain ranges where initiation was associated more with a grain boundary mechanism. A mixed mode of propagation with a faceted fracture morphology was typical for all cycle characters. Due to the plastic strain range being much less than the elastic one, pronounced opposite shift of mean stress occurred during hold time, which accounted quantitatively for the observed fatigue behavior. Compressive hold appeared more detrimental than tensile hold mainly due to its higher maximum tensile stress. The dependence of life on maximum tensile stress can be demonstrated by the data falling onto three lines corresponding to the three tensile hold times, in the life against maximum tensile stress plot. Consequently, the fatigue life models that hypothesize a deleterious creep-fatigue interaction tend to underpredict lives of tensile hold and overpredict in the case of compressive hold. In NARloy Z, crack initiation was always at the grain boundaries. The mode of crack propagation depended on the cycle character. It was transgranular mode for continous cyclong at high strain rate and for compressive hold. Intergranular propagation under continuous cycling at low strain rate was due to environmental effect and it was due to both creep and environmental effects for tensile hold tests. The life, therefore, decreased with decreasing strain rate and with tensile holds. In terms of damage mode, different life prediction laws may be applicable to different cycle characters, e.g., Coffin-Manson law to continuous hold, Coffin's frequency modified model to continuous cycling at low strain rate and SRP model to tensile hold.

17. Key Words (Suggested by Author(s)) Fatigue Life prediction High temperature Creep Creep-fatigue Microstructure	18. Distribution Statement Unclassified - unlimited STAR Category 26		
19. Security Classif. (of this report) Unclassified	20. Security Classif. (of this page) Unclassified	21. No. of Pages 110	22. Price* A06